Western diet induces iron-dependent enteric neurodegeneration via ferroptosis

Arun Balasubramaniam[1,2†], Dmitrii Pavlov[4†], Yunpeng Du[4], Jeremy Reeves[4], Alan Harzman[5], Yunshan Liu[1,2], Francesca Cingolani[1,2], Xinxu Yuan[6], Jay M. Patel[2,7], Simon Musyoka Mwangi[1,2], Peijian He[1], C. Michael Hart[2,3], Wenhui Hu[6], Fievos L. Christofi[4], Shanthi Srinivasan[1,2*]

[1]Division of Digestive Diseases, Emory University School of Medicine, Atlanta, GA, USA
[2]Atlanta VA Health Care System, Atlanta, GA, USA
[3]Division of Pulmonary, Allergy, Critical Care and Sleep Medicine, Emory University School of Medicine, Atlanta, GA, USA
[4]Department of Anesthesiology, The Ohio State University, Columbus, OH, USA
[5]Department of Surgery, The Ohio State University, Columbus, OH, USA
[6]Department of Neuroscience and Anatomy, Virginia Commonwealth University, Richmond, VA, USA
[7]Department of Orthopaedics, Emory University School of Medicine, Atlanta, GA, USA

Running title: Ferroptosis in the ENS

*Corresponding author email address: ssrini2@emory.edu (S.S)
Mailing address: 615 Michael Street NE, Atlanta, GA 30322
Tel.: +1-404-727-5638
Fax: +1-404-727-5767

†: Co-first authors contributed equally to this work.

Keywords: Enteric Nervous System (ENS), Ferroptosis, Palmitic Acid, Western Diet, networks of human Myenteric Plexus Ganglia (nhMPG).

Competing Interests
The authors declare no competing interests.

Abstract

Western diets (WD), high in saturated fats such as palmitic acid (PA), promote enteric neurodegeneration and motility disorders. Using murine models, *in vitro* systems, and human myenteric ganglia, we investigated whether WD and PA drive iron-dependent ferroptotic injury in the enteric nervous system. Mice were fed control diet (CD) or WD for 12 weeks, with or without systemic AAV9-MaCPNS2 delivery of Nfe2l2 to enteric neurons. Colonic motility was assessed by bead-expulsion assay. Ferroptosis was assessed using convergent readouts including iron dysregulation (TfR1, FTH-1, labile and mitochondrial Fe^{2+}), lipid peroxidation (C11-BODIPY and 4-HNE), GPX4 suppression, and pharmacologic inhibition by ferrostatin-1 (Fer-1) in primary enteric neurons, murine myenteric plexuses, and human networks of myenteric ganglia (nhMPG). WD-fed mice exhibited delayed colonic transit, increased TfR1 and FTH-1, and vulnerability of nNOS neurons; these changes were reversed by Nfe2l2 overexpression. RNA-seq of PA-treated IM-FEN neuronal cells revealed disrupted of neurotransmitter signaling, reduced mitochondrial and antioxidant programs, and increased iron import and lipid peroxidation signatures. PA increased labile iron, mitochondrial ROS, membrane depolarization, Ca^{2+} dysregulation, 4-HNE, and Mfrn2, while Fer-1 preserved mitochondrial integrity, viability, and ENS function. In human nhMPG, PA induced enteric neuronal iron loading and ferroptosis, supporting translational relevance to diet-associated enteric neuropathy.

Introduction

The enteric nervous system (ENS), a complex and autonomous network of neurons and glia embedded within the gastrointestinal (GI) tract, is essential for regulating gut motility, secretion, immune responses, and barrier function(1). Often referred to as the "second brain(2)," the ENS operates independently of the central nervous system (CNS), yet remains tightly integrated with systemic physiological cues(1, 3). Notably, its neuronal populations are largely post-mitotic, and exhibit limited regenerative capacity, rendering them particularly vulnerable to chronic metabolic insults(4, 5). In parallel with the global rise in obesity and metabolic syndrome, gastrointestinal symptoms such as constipation, altered motility, bloating, and discomfort are increasingly prevalent in affected individuals(6). Despite the high burden of GI dysfunction in these populations, the mechanisms linking diet-induced metabolic stress to enteric neuronal injury are not well understood. Studies suggest that disruptions in neuronal homeostasis within the myenteric plexus may underlie these symptoms(7), but the molecular underpinnings remain largely unexplored. Among dietary components, saturated fatty acids (SFAs) particularly PA are consistently associated with adverse metabolic and inflammatory outcomes(8). PA is not only a key contributor to lipotoxicity in peripheral tissues such as liver and adipose tissue but also induces oxidative stress and cell death in central and peripheral neurons(9, 10). Here we studied the role of iron overload in WD/PA-induced enteric neurodegeneration with a focus on ferroptosis. WD/PA disrupts ENS function, but the regulated death mechanism is unclear. We focused on ferroptosis since it is an iron-driven lipid peroxidation program and Nfe2l2 because it controls antioxidant and lipid-peroxide detoxification pathways that restrain ferroptotic susceptibility.

A growing body of research implicates ferroptosis, a form of regulated cell death distinct from apoptosis and necrosis, as a key mechanism of metabolic and neurodegenerative diseases(11). Ferroptosis is characterized by iron accumulation, lipid peroxidation, depletion of glutathione (GSH), and inactivation of glutathione peroxidase 4 (GPX4)(12). Mitochondrial dysfunction(13), redox imbalance, and failure to resolve reactive oxygen species (ROS) contribute to this cascade, ultimately leading to loss of membrane integrity and cell death(11). While ferroptosis has been documented in the CNS(14), its contribution to enteric neurodegeneration under high-fat dietary conditions has not been investigated. Moreover, enteric neurons are not the only ENS-resident cells susceptible to lipid stress. Enteric glial cells, which play critical roles in neuroprotection, neurotransmission, and inflammation, may also respond to oxidative injury and contribute to disease progression(15). The transcription factor Nfe2l2 (also known as Nrf2) serves as a central regulator of antioxidant defenses and cytoprotective gene expression. By activating antioxidant response elements (AREs), Nfe2l2 orchestrates cellular defense programs against oxidative and electrophilic stress(16). Prior studies have shown that loss of Nfe2l2 sensitizes neurons to ferroptosis(17), whereas pharmacologic or genetic activation of this pathway confers protection in various cell types(18, 19). However, whether Nfe2l2 plays a similar protective role in the ENS particularly under conditions of chronic lipid and saturated fatty acid (SFA) overload has not been determined.

In this study, we tested the hypothesis that WD and SFA's such as PA caused intestinal ENS neuropathy and disruption of motility by induction of ferroptosis in mice and humans and identified the underlying cellular and molecular mechanisms. We also explored whether Nfe2l2, a central regulator with antioxidant properties, could protect against damage of the ENS under conditions of chronic lipid overload. A comprehensive investigation characterized the effects of PA on enteric neurons using immortalized murine fetal enteric neurons (IM-FEN), primary enteric neuronal cultures, *in vivo* dietary models, and freshly isolated intact human neural networks of myenteric ganglia (nhMPG) from colectomy patients. In designing these experiments, we specifically focused on dietary lipid composition rather than obesity per se as the primary driver of ferroptotic injury.

PA triggered a ferroptosis-like injury program in the ENS, marked by increased iron import, reduced iron export, elevated labile iron and mitochondrial ROS, GPX4 suppression, lipid peroxidation and neuronal dysfunction Transcriptomic changes suggested altered neuronal identity and pathways linked to calcium and synaptic transmission supported by disruption in neuronal excitability and Ca^{2+}signaling. *In vivo*, AAV-mediated Nfe2l2 delivery to the myenteric plexus restored antioxidant signaling and improved motility in WD-fed mice, identifying Nfe2l2 as a therapeutic leverage point. Human nhMPG networks showed conserved PA-associated neuronal iron dysregulation, neuronal loss, and glial activation and studies support ferroptosis as a key translational mechanism of diet-related enteric neurodegeneration.

Results

Palmitic Acid Induces Ferroptosis and Iron Accumulation in Enteric Neurons

To investigate whether PA triggers ferroptotic stress in the ENS, we first evaluated the transcriptional and protein-level changes associated with iron metabolism and ferroptosis in murine enteric neurons. PA was used at 0.5 mM, consistent with our prior work showing this dose induces enteric neuronal degeneration(20). Also, PA is a major circulating fatty acid, and plasma measurements show that PA concentrations vary widely, from about 0.3 up to 4 mmol/L, placing 0.5 mM within the physiological range(21). Bulk RNA-seq of IM-FEN cells treated with PA (0.5 mM, 24h) revealed a marked upregulation of TfR1 (transferrin receptor 1), DMT1 (divalent metal transporter 1), and SLC39A14 (ZIP14), genes encoding major iron influx transporters (Figure 1A). Simultaneously, SLC40A1 (ferroportin), which facilitates cellular iron export, was downregulated, indicating a transcriptional shift toward iron retention. These changes suggest that PA promotes intracellular iron loading, a key trigger of ferroptosis.

Quantitative RT-PCR validated these RNA-seq findings, confirming elevated TfR1 ($p<0.001$), DMT1 ($p<0.001$), and pro-inflammatory cytokine IL-6 ($p<0.001$) as well as reduced GPX4 ($p<0.05$) and SLC40A1($p<0.001$) (Figure 1B). Western blot analysis demonstrated increased protein levels of FTH-1 ($p<0.001$), which stores excess iron(22, 23), and immunofluorescence of primary enteric neurons corroborated enhanced FTH-1 ($p<0.001$), TfR1 expression ($p<0.001$), and reduced enteric neuronal marker, class III β-tubulin (TUBB3, $p<0.01$), (Figure 1C-F). These results collectively indicate that enteric neurons respond to PA by activating iron uptake and storage-mechanisms hallmarks of ferroptotic priming. To determine whether this transcriptional shift results in functional iron overload, we assessed labile Fe^{2+} using FeRhoNox-1 staining. PA increased cytosolic Fe^{2+} ($p<0.05$) in IM-FEN cells, whereas co-treatment with the ferroptosis inhibitor Fer-1 reversed this accumulation ($p<0.05$) (Figure 1G). These findings establish that PA-induced ferroptosis in enteric neurons is initiated through iron dysregulation and is preventable through pharmacological inhibition.

Ferroptotic Stress Impairs Neuronal Identity via Oxidative Damage and Lipid Peroxidation

In addition to iron accumulation, we observed substantial neuronal degeneration in PA-treated IM-FEN cells. Bulk RNA-seq revealed that neuronal markers, including TUBB3 and PRPH (Peripherin), were downregulated, while oxidative stress-related genes were upregulated (Figure 2A-B). These transcriptional changes are consistent with reduced expression of neuronal markers and increased expression of stress-related genes, suggesting a shift in molecular signatures under ferroptotic stress. PA exposure led to a dramatic increase in propidium iodide (PI) ($p<0.001$) incorporation in IM-FEN cells, indicating plasma membrane rupture and cell death. Fer-1 reduced PI uptake ($p<0.01$), reinforcing the ferroptotic nature of this injury (Figure 2C). Immunofluorescence analysis of primary enteric neurons showed that PA elevated levels of Alox15 ($p<0.001$), a lipid peroxidizing enzyme that amplifies ferroptotic damage, and concurrently decreased GPX4 ($p<0.05$), the central antioxidant enzyme preventing lipid peroxide accumulation(12, 24)(Figure 2E-F). Lipid peroxidation was confirmed by increased 4-HNE ($p<0.001$) staining in neuronal soma and neurites (Figure 2G). Fer-1 rescued GPX4 expression ($p<0.01$) and suppressed both 4-HNE accumulation ($p<0.01$) and loss of neuronal markers (nNOS, $p<0.05$; TUBB3, $p<0.05$) (Figure 2D,F,G). Together, these findings support a model in which PA-induced iron accumulation drives lipid peroxidation, oxidative damage, and loss of enteric neurons through ferroptosis.

Palmitic Acid Impairs Mitochondrial Integrity and Triggers Mitochondrial Ferroptosis

To identify components of the ferroptotic stress response, we analyzed gene expression signatures in PA-treated IM-FEN cells. Transcriptomic profiling revealed upregulation of multiple heat shock proteins (HSPs), including Hspa1a, Hspa5, Hsp90aa1, Hspa8, and Hspb1 (Supplementary Figure 2A). These molecular chaperones play central roles in protein folding,

proteostasis, and the management of cellular stress, including stabilization of mitochondrial and cytosolic proteins under oxidative damage(25). HSPs also indirectly modulate ferroptosis by maintaining mitochondrial function and redox homeostasis(26). Most genes encoding subunits of mitochondrial Complex I (NADH:ubiquinone oxidoreductase) including Ndufaf3, Ndufaf4, Ndufab1, Ndufaf7, Ndufa10, and Ndufa4l2 were downregulated (Figure 3B). This suppression suggests mitochondrial dysfunction and impaired electron transport capacity in response to metabolic stress. Given the central role of Complex I in initiating oxidative phosphorylation, reduced expression of its components may reflect a collapse in mitochondrial bioenergetics and an adaptive attempt to limit further ROS production under conditions of ferroptotic stress.

Supporting this, PA also reduced the expression of Dhodh and Aifm2 (FSP1), two critical suppressors of ferroptosis that detoxify lipid peroxides via mitochondrial and plasma membrane CoQ(27, 28) (Figure 3A). These transcriptomic changes were functionally validated by MitoSOX Red staining, which revealed elevated mitochondrial ROS levels in PA-treated IM-FEN cells ($p<0.001$), which were attenuated by the ferroptosis inhibitor Fer-1($p<0.01$) (Supplementary Figure 9F). In addition, MitoFerroGreen imaging (co-labeled with MitoTracker) revealed a increase in mitochondrial labile Fe^{2+} following PA exposure, which was reduced by Fer-1 (Figure 3C), directly linking PA to mitochondrial iron loading during ferroptotic stress. Consistent with these findings, MitoBrilliant 646 imaging showed fragmented mitochondrial networks in primary enteric neurons, consistent with organelle depolarization and dysfunction ($p<0.01$) (Figure 3D). Expression of Mitoferrin-2 (Mfrn2), a mitochondrial iron importer(29), was also increased ($p<0.001$) (Figure 3E), suggesting enhanced mitochondrial iron accumulation a known amplifier of ferroptosis via Fenton chemistry.

Together, these findings indicate that PA triggers ferroptosis in enteric neurons by disrupting mitochondrial respiration, suppressing key ferroptosis inhibitors (FSP1, DHODH), and initiating oxidative and proteotoxic stress responses (via upregulation of HSPs). These transcriptional and functional changes converge on a mitochondria-centered ferroptotic pathway characterized by elevated ROS, iron dysregulation, and mitochondrial injury, which can be partially rescued by ferroptosis inhibition.

Ferroptosis inhibition separates acute physiological from chronic ferroptotic effects of PA on enteric neuronal Ca^{2+} signaling.

We next used Ca^{2+} imaging in IM-FEN enteric neurons to distinguish acute physiological effects of PA from chronic ferroptotic injury (Figure 4). Electrical field stimulation (EFS) evoked robust, frequency-dependent Ca^{2+}transients in Fluo-4-loaded IM-FEN cells, and the EFS frequency-response curve closely matched that recorded in neurons of intact LMMP preparations from Wnt1:GCaMP reporter mice, indicating that IM-FEN faithfully reproduces native enteric neuronal activity. TTX abolished EFS-evoked Ca^{2+} responses, confirming that these signals depend on Na_v-mediated action potential conduction (Figure 4A-C). Chronic exposure to 0.5 mM PA (24h) markedly suppressed EFS-evoked Ca^{2+}responses and functionally silenced neurons, whereas pretreatment with the ferroptosis inhibitor Fer-1 preserved the EFS frequency-response relationship despite chronic PA exposure (Figure 4A-C).

Acute PA exposure produced a distinct, non-lethal profile. Short-term perfusion with PA (2-10 min) alone induced agonist Ca^{2+}transients that were not affected by Fer-1 (Figure 4D) and did not cause measurable cell death by either propidium iodide or Trypan Blue exclusion, in contrast to chronic 0.5 mM PA, which killed more than 50% of IM-FEN neurons in a Fer-1-sensitive manner (Figure 4E; Supplementary Figure 9E). Acute PA also modulated EFS responses in a concentration-dependent manner: 0.1 mM PA strongly inhibited EFS-evoked Ca^{2+} signals, whereas 0.5 mM PA enhanced responses at low-intermediate stimulation frequencies and revealed a TTX-insensitive component (Figure 4F-H), suggesting recruitment of a TTX-resistant conductance. Fer-1 did not alter these acute effects (Figure 4H). Together, these data identify two mechanistically distinct phases of PA action in enteric neurons: a rapid, reversible, Fer-1-

insensitive modulation of Ca^{2+} signaling and a delayed, Fer-1-sensitive ferroptotic phase characterized by loss of neuronal activity and cell death.

PA Suppresses Phospho-Nfe2l2 and AAV-Mediated Nfe2l2 Overexpression Restores Redox Balance In Vivo

To determine whether PA disrupts endogenous antioxidant signaling, we assessed phospho-Nfe2l2 (p-Nfe2l2) levels in primary enteric neurons. PA treatment reduced nuclear p-Nfe2l2 expression ($p<0.001$), indicating impaired activation of this redox-responsive transcription factor(30). Bulk RNA-seq further confirmed that Nfe2l2 mRNA levels were downregulated by PA treatment in IM-FEN cells (Figure 1A). Co-treatment with Fer-1 restored p-Nfe2l2 levels ($p<0.001$), suggesting that ferroptotic stress directly suppresses Nfe2l2 signaling (Figure 5A). Transcriptomic profiling revealed that PA altered key regulators of lipid metabolism, inflammation, and gastrointestinal motility. Genes such as Srebf2, Insig1, Insig2(31), and Nr3c1(32) were upregulated, and Ucp2(33) was downregulated (Supplementary Figure 2B), suggesting a shift toward enhanced lipid and steroid regulatory signaling alongside compensatory and impaired mitochondrial lipid utilization. Concurrently, PA upregulated inflammatory mediators (Tlr4(34), Myd88, Nfkb1(35)) and motility-related neuromodulators (Gabra1(36), Adra2a(37), Cnr1(38), Nts(39)) (Supplementary Figure 2C), indicating activation of neuroimmune pathways and inhibitory neurotransmission that may collectively disrupt enteric neuronal function and gastrointestinal transit. To assess the functional relevance of Nfe2l2 in vivo, we used the AAV-MaCPNS2 capsid, which efficiently transduces peripheral neurons, including enteric neurons, to drive Nfe2l2 expression in adult mice (Figure 5B). Notably, AAV-MaCPNS2 is not selective for myenteric neurons over other peripheral ganglia. We selected a 12-week feeding paradigm because our prior work established this as the earliest-time point at which enteric neurodegeneration and delayed colonic transit are detected (40). To confirm successful AAV-mediated gene delivery, we assessed transduction efficiency one week after AAV injection (week 3 of the 12-week experiment). eGFP fluorescence was observed in the colonic myenteric plexus by whole-mount confocal imaging, and qRT-PCR of colon tissue enriched for the myenteric plexus confirmed an increase in Nfe2l2 mRNA expression in AAV-Nfe2l2-treated mice compared to AAV-eGFP controls (Supplementary Figure 3A, B). At the experimental endpoint (week 12), immunofluorescence staining of colon tissue sections showed sustained upregulation of total and phospo-Nfe2l2 protein in enteric neurons, with strong co-localization with the neuronal marker TUBB3 and elevated t-Nfe2l2 and p-Nfe2l2 fluorescence intensity in the AAV-Nfe2l2 group ($P<0.001$; Figure 5C and Supplementary Figure 13). AAV-mediated overexpression of Nfe2l2 improved colonic motility in WD-fed mice, as assessed by bead expulsion time. WD feeding delayed motility in both sexes compared to controls ($p < 0.05$). Nfe2l2 overexpression prevented the delayed motility induced by Western diet in both males and females (Figure 5D, E). These results support a functional role for Nfe2l2 in restoring gastrointestinal motility under WD-induced metabolic stress. Collectively, these findings demonstrate that PA/WD suppresses Nfe2l2 signaling in enteric neurons, contributing to ferroptosis and motility impairment. AAV-mediated overexpression of Nfe2l2 reestablishes redox homeostasis and improves gastrointestinal function in the context of WD-induced metabolic dysfunction.

Western Diet Induces Ferroptotic Signaling and Compromises ENS

To assess the long-term effects of Western diet (WD) on enteric neuronal ferroptosis, we analyzed colonic tissues from mice that fed either a control diet (CD) or WD for 12 weeks. AAV vectors (eGFP or Nfe2l2) were administered at week 2 to enable targeted modulation of antioxidant signaling in enteric neurons. WD-fed mice exhibited the characteristic pattern of progressive weight gain over time compared to CD-fed controls, confirming progressive diet-induced obesity (Supplementary Figure 2D,E). Immunofluorescence analysis revealed that WD exposure notably increased expression of transferrin receptor 1 (TfR1, $p<0.001$) and ferritin heavy

chain (FTH-1, $p<0.001$) within myenteric ganglia compared to CD-fed controls (Figure 6A-B), indicating chronic iron accumulation and sustained ferroptotic stress. These changes mirror those observed in PA-treated enteric neurons (Figure 1) and suggest that dietary lipotoxicity activates ferroptotic programs *in vivo*. Notably, AAV-Nfe2l2 overexpression markedly suppressed both TfR1 (Male, $p<0.05$; Female, $p<0.001$) and FTH-1 (Male, $p<0.01$; Female, $p<0.05$) expression, reinforcing the role of Nfe2l2 in regulating neuronal iron metabolism and mitigating ferroptotic signaling.

Concurrently, we observed suppression of key neuronal and redox associated markers in WD-fed animals. nNOS- a critical enzyme for nitrergic neurotransmission and gut motility was significantly downregulated (Male, $p<0.05$; Female, $p<0.01$) in WD-fed mice, indicative of neuronal dysfunction (Supplementary Figure 4). Collectively, these findings demonstrate that chronic consumption of a WD exacerbates iron overload and ferroptosis-associated molecular injury in the ENS, while simultaneously impairing nitrergic signaling and antioxidant defense. Importantly, AAV-Nfe2l2 gene therapy both limits ferroptotic stress and partially restores neuronal function, highlighting its translational potential as a neuroprotective strategy in the context of metabolic stress-induced enteric neuropathy.

To assess whether ferroptotic stress markers localize to specific enteric neuronal subtypes, we co-labeled myenteric ganglia for TUBB3 with nNOS, ChAT, or TH together with 4-HNE and DRP1 (Supplementary Figures 10-12). Western diet increased 4-HNE and DRP1 signals across all three neuronal populations, without a consistent subtype hierarchy. The clearest subtype-associated separation *in vivo* was observed in female $ChAT^+$ neurons. In parallel, PA exposure in primary ENS cultures induced a comparable 4-HNE and DRP1 stress signature across $nNOS^+$, $ChAT^+$, and TH^+ neurons (Supplementary Figure 8C). Fer-1 attenuated these PA-induced changes, supporting lipid peroxidation as a central component of the neuronal stress response. Together, these data indicate that WD and PA engage broadly shared ferroptotic stress across myenteric neuronal subtypes, while subtype-selective vulnerability likely reflects downstream sensitivity rather than differential induction of these markers.

PA-Associated Ferroptosis Modulates Transcripts in Synaptic and Calcium Signaling Pathways in Enteric Neurons

To assess how PA-associated ferroptosis might influence neuronal signaling programs, we performed bulk RNA-seq on IM-FEN cells treated with PA or vehicle. Transcriptomic analysis revealed that genes annotated to calcium signaling and synaptic neurotransmission pathways were modulated following PA treatment (Supplementary Figure 1A-D). The purinergic receptor P2rx6, a key mediator of calcium influx (41), was downregulated, suggesting potential alterations in calcium handling under oxidative stress. Presynaptic genes essential for vesicle docking and release, including Rab3a(42) and Stx1b(43), also showed reduced expression, and glutamatergic signaling components such as Grm3 and Grm5(44) were downregulated.

These transcriptomic changes precede overt cell death and likely represent early stress responsive remodeling of neuronal signaling pathways during ferroptotic stress. We interpret these findings as hypothesis generating signatures that point to potential alterations in calcium handling and synaptic programs, rather than definitive evidence of functional impairment. Indeed, calcium imaging studies described earlier (Figure 4) support the hypothesis that PA induced transcriptional changes may underlie functional impairment in ENS and motility. Future studies are needed to test this hypothesis.

Human Myenteric Neurons Exhibit Conserved Ferroptotic Responses to Palmitic Acid

To determine whether PA-induced ferroptotic mechanisms observed in murine models are conserved in the human ENS, we freshly isolated networks of intact human myenteric ganglia (nhMPG) from 14 surgical intestinal specimens from patients undergoing elective colectomy.

These neural networks, an *in vitro* model of the human ENS, were treated with PA (0.5 mM for 24h) and analyzed using high-resolution confocal imaging to evaluate ferroptosis.

Patient metadata are summarized in Supplementary Table 4, including sex, age, BMI (mean 33.18 ± 6.74), diabetes status, clinical lab values (iron indices, lipid profile, HbA1c, CRP), medications, and surgical indications. Patients exhibited diverse metabolic and inflammatory profiles. Some were obese, had Type 2 diabetes (T2D), or exhibited impaired fasting glucose (IFG); others had normal metabolic panels. A subset showed altered systemic iron metabolism e.g., one patient with high ferritin, another with elevated transferrin saturation and a few had elevated CRP, indicating low-grade inflammation. Despite this variability, all nhMPG preparations exhibited PA-induced ferroptotic phenotypes, underscoring the generalizability of this mechanism in the human colon.

After standardization of isolation protocols (Supplementary Figure 5A), nhMPG networks were maintained under optimized conditions in organotypic culture medium in a humidified 5% CO_2 chamber to permit treatment with PA or other agents. preserving ganglionic integrity and functionality. Networks remained suspended in medium during PA exposure, minimizing any glial/cell differentiation unrelated to PA induction. Transmitted light imaging showed well-preserved architecture and diverse morphologies across patients, with clearly delineated ganglia and neurite projections (Supplementary Figure 5B).

Upon PA exposure, widespread cell death was observed in HuC/D$^+$ neurons, marked by robust PI uptake compared to vehicle-treated controls (Figure 7A-D). Quantitative analysis revealed a 12.1-fold increase in PI$^+$/HuC/D$^+$ nuclei per field, a 5.5-fold increase in colocalization area, and a 1.46-fold increase in PI fluorescence intensity ($p < 0.001$; Figure 6E). PA also triggered nuclear translocation of HuC/D (Figure 7F), a known stress marker, and caused a 28% reduction in neuronal density ($p < 0.001$; Figure 7G). Notably, while HuC/D fluorescence intensity declined slightly in some fields (Figure 7H), this may reflect complete loss of heavily damaged neurons. Z-stack cross-sections demonstrated pronounced architectural disruption and fragmented nuclei (Figure 7I), mirroring murine data and validating the ferroptotic phenotype in human tissue.

TfR1 is Upregulated in Neuronal and Non-Neuronal Compartments of Human nhMPG Networks Following PA, FAC, and LPS Exposure

Given the centrality of iron in ferroptosis, we next analyzed a prominent marker of ferroptosis is transferrin receptor-1 that transports iron into cells, resulting in elevated labile iron levels that can potentially cause toxicity(45). TfR1 and co-labeling studies evaluated the effect of PA on TfR1 expression in human enteric ganglia. PA increased TfR1 expression in HuC/D+ neurons of nhMPG networks, compared to DMEM or vehicle control (with BSA, Figure 8A-E); Data analysis showed that PA caused an increase in the number of neurons/field that expressed TfR1 (Figure 8F, $p<0.01$), and it increased the area of co-localization of TfR1 and HuC/D+ neurons/field (Figure 8G, $p<0.01$). Expression of TfR1 (pixel intensity) for TfR1 immunoreactivity in neurons/field was also increased by PA treatment (Figure 8H, $p<0.05$).

To contextualize this response, we compared PA to known ferroptosis inducers such as ferric ammonium citrate (FAC), a strong stimulus for induction of ferroptosis(46), caused a huge upregulation of TfR1 in neurons of nhMPG networks (Supplementary Figure 6A-D). The bacterial membrane toxin LPS (1µg/ml) also caused TfR1 upregulation in enteric neurons (Supplementary Figure 6E-G). Secondary data analysis was done to compare PA, LPS and FAC in inducing TfR1 expression in nhMPG networks. Data is summarized in Supplementary Figure 6H and 6I. A concentration of 0.5mM PA ($p<0.05$) or 1µg/ml LPS induction ($p<0.05$) for 24h caused the same level of upregulation in the neuronal TfR1 expression/field ($p>0.05$ for the difference). FAC caused a several fold higher level of TfR1 expression in neurons/field compared to LPS or PA (Supplementary Figure 6H). PA induced TFR1 expression in nhMPG networks in about 20% of the neuronal population induced with FAC (FAC >> PA, $p<0.001$). In contrast, a secondary analysis, for non-neuronal TfR1 expression (based on indirect analysis of TfR1 expression in

areas not co-labeled with the neuronal marker HuC/D) showed that PA induction of TFR1 in non-neuronal cells >> FAC ($p<0.001$); differences were observed for both total area/field labeled for TfR1 (Supplementary Figure 6I) or number of different areas/field labeled for TfR1 ($p<0.001$, Supplementary Figure 6J) immunoreactivity. Pixel intensity was marginally but significantly higher with FAC > PA ($p<0.001$, Supplementary Figure 6K).

PA induction of FTH-1 expression in human myenteric neurons of nhMPG networks

To further assess iron-handling responses in human ENS under lipid stress, we examined expression of ferritin heavy chain (FTH-1), the primary intracellular iron storage protein and a key ferroptosis marker. Following 24h PA treatment, FTH-1 was robustly upregulated in human nhMPG networks. Immunofluorescence analysis revealed an 11.3-fold increase in the number of FTH-1$^+$/HuC/D$^+$ neurons per field and a 1.5-fold increase in average signal intensity within these neurons ($p< 0.001$; Figure 9A-G). Morphologically, FTH-1 localized prominently within the somatic cytoplasm and proximal neurites of stressed neurons.

Importantly, FTH-1 expression was also elevated in non-neuronal regions of the network, including glial-like territories not co-labeled with HuC/D. Quantification showed increased FTH-1 signal area, number of labeled regions, and intensity across these compartments ($p<0.001$; Figure 9H-J), indicating that the iron sequestration response was not restricted to neurons but extended throughout the ENS microenvironment. This widespread FTH-1 upregulation may represent an adaptive buffering mechanism against rising intracellular labile iron but also reflects ongoing iron dysregulation and ferroptotic pressure. These findings parallel murine data, reinforcing FTH-1 as a robust marker of ferroptotic stress in both neurons and glia.

PA induced disruption of morphology and activation of glial GFAP in nhMPG networks

In addition to neuronal ferroptosis seen in all 14 patients, we examined whether glial cells and network architecture were affected by PA treatment. Although most nhMPG networks retained structural integrity, 2 out of 14 patient-derived preparations exhibited overt ganglionic disorganization and morphological collapse following PA exposure. Co-staining with HuC/D, DAPI, and PI revealed loss of organized ganglionic boundaries, fragmented neuronal nuclei, and diffused PI signal, indicative of both necrotic and ferroptotic processes (Supplementary Figure 7A-B). This observation suggests that ferroptosis may progress in some cases from isolated cellular injury to structural breakdown of the entire ganglionic unit.

To evaluate glial stress responses, we analyzed expression of glial fibrillary acidic protein (GFAP), a hallmark of reactive gliosis. GFAP is typically absent or minimally expressed in healthy human enteric glia but is strongly induced under inflammatory or degenerative conditions. Following PA treatment, GFAP was clearly upregulated in enteric glial regions of the nhMPG ($p<0.001$; Supplementary Figure 7C), indicating activation of gliotic remodeling programs in response to lipid-induced stress. Together, these findings demonstrate that ferroptotic injury in the human ENS extends beyond neuronal death to include glial reactivity and, in more severe cases, network-level disruption. This dual cellular involvement highlights the broader pathogenic impact of saturated lipid overload on ENS integrity and function.

Discussion

This study defines PA- and WD-induced ferroptosis as a principal, conserved mechanism of enteric neurodegeneration, with direct relevance to gastrointestinal (GI) dysfunction observed in metabolic diseases such as diet-induced obesity. By leveraging murine models, *in vitro* enteric neuronal cultures, and human myenteric ganglia networks (nhMPG), we delineate a ferroptotic cascade characterized by iron dyshomeostasis, mitochondrial dysfunction, lipid peroxidation, and neuronal degeneration culminating in neurodegeneration of the ENS (Figure 10). While ferroptosis is well characterized in the CNS, particularly in stroke(47) and neurodegeneration models(48), its role in the ENS has been largely unexplored. The importance of our study lies in

filling this critical knowledge gap: identifying ferroptosis as a major pathophysiological mechanism of neurodegeneration in the ENS and establishing direct links between dietary lipid stress (PA and WD) and ferroptotic injury. Given the ENS's pivotal role in regulating GI motility and homeostasis, and the increasing incidence of GI complications in metabolic diseases, these findings have substantial clinical and translational relevance. We therefore examined mice after 12 weeks of WD, when colonic neurodegeneration and motility delay are established, to isolate diet driven ferroptotic mechanisms. *In vivo*, dietary PA is absorbed and metabolized, and WD induced enteric neurodegeneration likely reflects the combined actions of multiple circulating lipids and metabolites rather than PA alone. Thus, direct PA exposure *in vitro* serves as a reductionist model to define neuron intrinsic ferroptotic mechanisms of a WD associated saturated fatty acid, whereas WD feeding establishes *in vivo* relevance within the full metabolic and microbial context.

We observed that core ferroptotic processes iron overload, mitochondrial dysfunction, lipid peroxidation, and antioxidant failure are conserved between CNS and ENS, confirming ferroptosis as a broadly conserved mechanism of neuronal injury. Consistent with its well-established cytoprotective role in CNS disorders, FTH1 is traditionally considered cytoprotective by buffering labile Fe^{2+}(49), our findings in ENS highlight a more nuanced and context-specific regulation of FTH1 in the setting of PA-induced ferroptosis. Although canonical FTH1 mRNA expression was modestly downregulated in our model, FTH1 protein levels were robustly elevated. This apparent disconnect may be explained by upregulation of FTH1-ps2, a pseudogene known to act as a competing endogenous RNA (ceRNA), stabilizing FTH1 mRNA by sequestering inhibitory miRNAs (50). In addition, iron regulatory proteins (IRPs) may facilitate translational derepression of FTH1 under iron overload conditions(51). Therefore, the observed FTH1 protein upregulation likely reflects a stress-adaptive response to excess iron rather than a protective mechanism sufficient to prevent ferroptosis. Notably, ferritin induction does not universally confer ferroptosis resistance, under certain conditions, ferritin instability or ferritinophagy can paradoxically exacerbate oxidative stress. Thus, FTH1 upregulation in our model may signal ferroptotic stress without necessarily abrogating it. Beyond its role in lipotoxicity and ferroptosis, PA also serves as a substrate for S-palmitoylation, a reversible lipid modification that regulates the localization and function of many neuronal proteins. Although palmitoylation was not assessed here, PA-driven changes in protein palmitoylation may represent an additional mechanism contributing to ENS dysfunction in high-fat states and will require dedicated investigation.

Prior studies have reported that enteric glia outnumber neurons by approximately 7:1, providing important structural context(52). In our experimental models, enteric glia were highly susceptible to ferroptotic stress, as evidenced by TfR1 upregulation and de novo GFAP expression following PA exposure. Glial ferroptosis likely amplifies neuronal injury, highlighting neuron-glia crosstalk as a critical driver of ferroptotic damage in the ENS. In epilepsy, reactive astrocytes can modulate neuronal ferroptosis through chemokines; for example, astrocyte-derived CXCL10 acting via CXCR3 promotes neuronal ferroptosis (53). These CNS data support the broader concept that diverse reactive glial states, rather than discrete A1/A2 categories, can shape neuronal vulnerability to ferroptosis, a framework that is likely to extend to enteric glia as well (54). Astrocytes in the setting of inflammation can trigger ferroptosis in neurons by releasing chemokines and cytokines like IL-6 that in turn can induce expression of proteins like ferroportin in neurons leading to ferroptosis. In addition, astrocytes through Nfe2l2 can counter neuronal ferroptosis by releasing exosomes(55). The interaction between glia and neurons in the enteric nervous system has to be further examined. Interestingly, although Nfe2l2 is canonically known to transcriptionally activate FTH1(56), we observed a reduction in FTH1 protein levels upon Nfe2l2 overexpression during WD exposure. This does not imply direct repression of ferritin genes but rather suggests that Nfe2l2 activation limits the upstream ferroptotic stimuli namely iron influx and oxidative stress that drive compensatory FTH1 induction. By restoring iron and redox

homeostasis, Nfe2l2 indirectly reduces the cellular need for ferritin-based iron sequestration. This context-dependent regulation reinforces Nfe2l2's role in suppressing ferroptotic signaling and highlights its potential therapeutic relevance in the ENS.

Our study provides several key findings: (1) identification of PA and WD as potent inducers of ferroptosis-driven enteric neurodegeneration in both murine and human ENS; (2) demonstration that Nfe2l2 activation restores redox balance, suppresses iron burden, preserves nitrergic neuronal identity (nNOS), and improves GI motility under WD stress; Consistent with this, phospho-Nfe2l2 immunostaining in colonic myenteric neurons confirms effective pathway activation after AAV-Nfe2l2 administration, and subtype-specific analyses showed broad induction of mitochondrial and ferroptotic stress across nNOS+, ChAT+, and TH+ neurons. and (3) cross-species validation showing that human nhMPG networks display conserved ferroptotic signatures, including neuronal death, TfR1/FTH-1 upregulation, HuC/D nuclear translocation, and glial activation. Dose response experiments in nhMPG further showed graded induction of neuronal TfR1 and FTH-1 together with progressive neuronal loss after PA exposure, indicating that saturated fatty acid driven iron loading and ferroptotic vulnerability are quantitatively conserved in human enteric neurons. Furthermore, we identified enhanced mitochondrial iron import via upregulation of mitoferrin-1 (Mfrn1) and mitoferrin-2 (Mfrn2) in enteric neurons, a distinct mechanism contributing to ferroptotic vulnerability through mitochondrial Fe^{2+} accumulation and oxidative stress.

Mechanistically, bulk RNA-seq of IM-FEN neurons exposed to PA revealed upregulation of iron importers (TfR1, DMT1, ZIP14) and downregulation of ferroportin (SLC40A1), leading to labile iron accumulation, as visualized by FeRhoNox-1 fluorescence. Despite FTH-1 upregulation, iron buffering was insufficient to prevent lipid peroxidation, as evidenced by increased 4-HNE levels. PA treatment downregulated mitochondrial Complex I subunits (Ndufa2, Ndufa4, Ndufa3) and antioxidant enzymes (Dhodh, FSP1), leading to elevated mitochondrial ROS production and disrupted membrane potential. Upregulation of Mfrn1,2 further facilitated mitochondrial iron import, exacerbating oxidative stress and ferroptotic injury. ER stress genes (Hspa1a, Hspa5, Hsph1) were concurrently induced, supporting a model of multi-organelle dysfunction. This pattern supports a biphasic response in which PA initially induces adaptive stress programs, including HSP pathways, but sustained exposure overwhelms GPX4- and Nfe2l2-dependent defenses so that residual protection is insufficient to prevent progression of ferroptosis. A complementary PA time course (4, 8, 12, 24h) in enteric neurons showed that early induction of TfR1 and IL-6 together with loss of FSP1 and GPX4 precedes major loss of viability, indicating that 24h PA exposure captures a mechanistically relevant ferroptotic endpoint rather than late nonspecific cell death. The integration of MitoFerroGreen/MitoTracker imaging, C11-BODIPY lipid peroxidation assays, and 4-HNE/DRP1 immunostaining links these transcriptional changes to mitochondrial Fe^{2+} loading, membrane damage, and structural stress, while Ca^{2+} imaging shows that chronic PA exposure converts early, reversible changes in excitability into a delayed, ferroptosis-associated loss of neuronal function. *In vivo*, AAV9-mediated overexpression of Nfe2l2 suppressed WD-induced iron overload, preserved nNOS+ neuronal populations, and restored colonic transit time, demonstrating the therapeutic potential of enhancing antioxidant defenses. These protective effects are supported by increased phospho-Nfe2l2 staining in distal colonic myenteric neurons after AAV-Nfe2l2 treatment. Human nhMPG networks from diverse patients recapitulated murine findings, with PA-induced neuronal death, nuclear HuC/D translocation, TfR1/FTH-1 upregulation, and glial GFAP induction, underscoring the clinical relevance of ferroptosis in human enteric neuropathy. Together, the murine and human datasets converge on a coherent ferroptotic signature that spans iron import, lipid peroxidation, mitochondrial injury, transcriptional remodeling, and functional neuronal failure.

In this study, bead expulsion testing and all histological and molecular analyses were performed on distal colonic segments, aligning functional and mechanistic readouts while acknowledging that mitochondrial and ferroptotic changes may vary along the gastrointestinal tract and will require future regional mapping. Although our murine and ex vivo models recapitulate key features of ferroptosis, *in vivo* complexity involving microbiota, immune modulation, and epithelial interactions remains to be explored. In this context, WD driven dyslipidemia, low grade mucosal inflammation, immune cell and glial activation, and microbiota derived metabolites are best viewed as converging inputs that collectively amplify oxidative and iron stress within the ENS rather than as isolated parallel pathways. Prior work in this WD model has already shown broad shifts in triglyceride species, bile acids, and microbial products, and these additional metabolites may further modulate ferroptotic susceptibility and will require targeted metabolomics in future studies(40). In addition, future studies will investigate how fat malabsorption and disrupted fluid drainage in the GI tract influence ferroptotic susceptibility and contribute to ENS dysfunction. Although our WD and human nhMPG data show glial iron loading, GFAP induction, and network disruption, the current study does not dissect causal neuron-glia interactions in ferroptosis or motility, which will require glia-targeted ferroptosis manipulation, neuron-glia co-culture systems, and spatial transcriptomics in WD-fed mice. Longitudinal human sampling, metabolic phenotyping, and bulk and single-cell transcriptomics of purified nhMPG networks will be essential to dissect cell-type-specific vulnerabilities. Electrophysiological recordings may further elucidate functional impairments within the enteric network during ferroptotic stress.

In conclusion, this study identifies ferroptosis as a principal, conserved yet distinct mechanism of enteric neurodegeneration triggered by PA and WD-induced lipid stress leading to abnormal motility. We demonstrated that dietary lipotoxicity disrupts iron homeostasis, impairs mitochondrial antioxidant defenses, promotes lipid peroxidation, and induces enteric neuronal and glial death in murine and human ENS. Enhanced mitochondrial iron loading and glial ferroptotic susceptibility emerge as unique amplifiers of injury in the ENS. Therapeutic activation of Nfe2l2 via AAV gene therapy represents a promising strategy to mitigate ferroptotic injury and preserve gastrointestinal function. These rescue experiments indicate that enhancing Nfe2l2 signaling is sufficient to reverse key WD induced ferroptotic changes, but do not imply that Nfe2l2 down regulation is the sole mediator of pathology. These findings provide critical mechanistic insight into enteric neuropathy in metabolic diseases and establish ferroptosis as a novel, translationally relevant and potential therapeutic target in human ENS disorders associated with abnormal motility.

Materials and Methods

Sex as a Biological Variable.

Experiments included male and female mice, and sex-stratified analyses were performed where indicated. Human colectomy-derived myenteric ganglia networks included donors of both sexes; sex-stratified analyses were not performed for human tissues.

Ethics Approval

Animal procedures were approved by the Atlanta VA Medical Center IACUC and followed ARRIVE guidelines. Human tissues were obtained under OSU IRB approval (OSU-IRB #2020H0273 and #2024H0125) with informed consent.

Animal and Diet

Male and female C57BL/6J mice (6 weeks old; Jackson Laboratories, Bar Harbor, ME, USA) were randomized to receive either a control diet (CD; TD.140305, 16.9% kcal from fat) or a Western diet (WD; TD.140304 34.5% kcal from fat) for 12 weeks (Teklad Diets, Envigo, Madison, WI, USA). Body weight was monitored weekly. At week 2, mice received a single retro-orbital

injection (I.V.) of AAV-MaCPNS2 capsid packaged with either pAAV-CMV-eGFP or pAAV-CMV-Nfe2l2-P2A/EGFP using 3-plasmid transfection system (VectorBuilder Inc., Chicago, IL, USA), delivering either 5×10^{11} or 1×10^{13} viral genomes per mouse. Mice were euthanized at week 12, and distal colonic segments corresponding to the region assessed by the bead assay were collected for downstream molecular and histological analyses.

Colonic Transit Measurement

Distal colonic transit was assessed at week-11 using the bead expulsion test(34) briefly described in supplemental methods.

Primary Enteric Neuronal Cell Isolation and Culture

Myenteric neurons were isolated from the intestines of male and female C57BL/6J mice aged 8-12 weeks, following previously established protocols(20). Cells were plated on Matrigel-coated chamber slides or 6-well plates and treated for 24h with vehicle (BSA), Fer-1 (10 μM), PA (0.5 mM), or PA+Fer-1. (See Supplemental Methods for details).

Culture and Treatment of Mouse Enteric Neuronal Cell Line

IM-FEN cells(57) were maintained and differentiated under established conditions and then treated for 24h with vehicle (BSA), Fer-1 (10 μM), PA (0.5 mM), or PA+Fer-1. (See Supplemental Methods for details).

Ca^{2+} imaging

Ca^{2+}imaging on electrical field stimulation (EFS) was done in the IM-FEN enteric neuronal cell line. Suitability of responses was confirmed in Wnt-1^{Cre2}:GCaMP5g-tdT Ca^{2+}reporter mice (58). Fluo-4/AM loading and imaging was described previously (59). Cells or LMMP preparations were perfused with oxygenated Krebs solution containing vehicle, PA (0.01-0.5 mM), Fer-1, or TTX, and time-series fluorescence was recorded during EFS across a range of frequencies. (See Supplemental Methods for details).

Immunofluorescence Staining and Imaging of Myenteric Neurons

Primary enteric neuronal cells were fixed for 20 min at RT in 4% paraformaldehyde in phosphate-buffered saline (PBS) and permeabilized at 4°C for 15 min with 0.3% Triton-X 100. The cells were then blocked with 5% Bovine Serum Albumin (BSA) in PBS for 1h and incubated overnight at 4°C with gentle shaking. A list of primary antibodies and their working dilutions is provided in Supplementary Table 1. After overnight incubation, the cells were incubated for 1h at RT with a secondary antibody (Supplementary Table 2). Nuclei were labeled with 4,6-diamidino-2-phenylindole (DAPI, Molecular Probes, Eugene, OR, USA). Cells were then mounted in Prolong Gold antifade mounting medium (Invitrogen, Eugene, OR, USA) and visualized using an Olympus IX51 microscope (Olympus, Tokyo, Japan) equipped with cellSens Standard 1.12 imaging software for fluorescence imaging or Nikon A1R equipped with NIS Elements software for confocal imaging. At least 5 fields were examined per group, and all experiments were replicated a minimum of three independent times.

FeRhoNox-1 Staining

IM-FEN enteric neuronal cells were cultured for 24h with PA (PA, 0.5 mM) or vehicle, with or without Fer-1. To assess labile iron levels, cells were incubated with 5 μM FeRhoNox-1 (Goryo Chemical, Sapporo, Japan) for 30 min at 39°C in the dark. Following incubation, cells were washed with PBS to remove unbound FeRhoNox-1. Fluorescence was captured using a Cytation C10 imaging system (Agilent Technologies, Santa Clara, CA, USA), and intensity was quantified using ImageJ to determine labile iron levels.

Propidium Iodide Staining

Cell viability was evaluated using the ReadyProbes Cell Viability Imaging Kit (Blue/Red, Cat. #R37108, ThermoFisher Scientific, Waltham, MA, USA) following 24-h treatments with PA, 0.5 mM; Sigma-Aldrich, vehicle (10% BSA; Sigma-Aldrich), Fer-1, 10 μM, or a combination of PA+Fer-1. (See Supplemental Methods for details).

Immunohistochemistry (IHC) Staining and Imaging of Myenteric Ganglia

Paraffin-embedded intestinal sections (10 μm) were deparaffinized, rehydrated, and subjected to heat-mediated antigen retrieval. Sections were blocked in 5% BSA and incubated overnight at 4°C with primary antibodies (Supplementary Table 1), followed by fluorophore-conjugated secondary antibodies for 1h at room temperature (Supplementary Table 2). Nuclei were counterstained with DAPI, and slides were mounted with antifade medium. See Supplemental Methods for details. Fluorescent images were acquired using a Nikon A1R confocal microscope (Nikon Instruments, Melville, NY, USA) with NIS Elements software. From each mouse, 6-10 randomly selected myenteric ganglia were imaged for quantification. Within each experiment, control and treated sections were imaged in the same session using identical confocal acquisition settings (laser lines, laser power, detector gain, offset, pinhole, scan speed, frame size, and zoom). Image analysis was performed using ImageJ software (NIH, Bethesda, MD, USA). The neuronal area, demarcated by TUBB3 immunoreactivity, was defined as the region of interest (ROI), and fluorescence intensity of the target protein was quantified within this ROI. For each marker, a single intensity threshold and analysis pipeline were defined a priori and applied uniformly to all images from that experiment. Data were normalized to the mean fluorescence intensity of the vehicle-treated control group and expressed as fold change in relative neuronal gene expression.

Human Tissue Collection and nhMPG Isolation

The human tissue collection, nhMPG isolation procedure and timeline are illustrated in Supplemental Figure 5A, and networks of myenteric ganglia are shown in Supplemental Figure 5B. The isolation technique was revised from Grundmann et al. (2015) (60) and nhMPG networks were shown to contain viable neurons and glia in electrophysiological recordings in our laboratory(61). (See Supplemental Methods for details).

Ex Vivo Treatments and Immunostaining of nhMPG

Human networks of myenteric ganglia (nhMPG) were isolated from surgical colonic specimens and kept in DMEM/F12 medium for the duration of the study. To assess ferroptotic stress and neuronal injury, isolated nhMPG tissues were treated ex vivo for 24h at 37°C in a humidified 5% CO_2 incubator with either PA 0.25mM, 0.5mM; Sigma-Aldrich, ferric ammonium citrate (FAC; 100 μM; Sigma-Aldrich), or lipopolysaccharide (LPS; 1 μg/mL; Sigma-Aldrich). Vehicle-treated controls received DMEM or 10% BSA in DMEM.

Quantitative Real-Time PCR (qRT-PCR) and Bulk RNA Sequencing

Total RNA was isolated, and reverse transcribed for TaqMan-based qRT-PCR. Relative gene expression was calculated by the 2^-ΔΔCt method with normalization to 18S rRNA or HPRT1; assay probe IDs are listed in Supplementary Table 3. For bulk RNA-seq, IM-FEN cells were treated with vehicle or PA (0.5 mM) for 24h (n = 6 per group) and processed for transcriptomic profiling by Novogene. (See Supplemental Methods for details).

Western Blotting

Enteric neuronal lysates were analyzed by SDS-PAGE and immunoblotting using standard procedures. Membranes were probed for FTH-1 with β-actin as loading control, and band intensities were quantified by densitometry. (See Supplemental Methods for details).

Measurement of Mitochondrial Integrity Using MitoBrilliant 646

To assess mitochondrial membrane integrity, primary enteric neuronal cells were treated with vehicle (Veh), Fer-1, PA; 0.5 mM, or a combination of PA and Fer-1 (PA+Fer-1) for 24h at 37°C in 4-well chamber. After treatment, cells were incubated with 100 nM MitoBrilliant 646 (Cat. #7700, Bio-Techne, Minneapolis, MN, USA) for 1h at 37°C in the dark. Cells were then fixed with ice-cold 4% PFA for 20 minutes and washed with PBS. Following fixation, cells were immunostained with the neuronal marker TUBB3 (Cat. #TUJ-0020, Aves Labs, Davis, CA, USA) and counterstained with DAPI (Molecular Probes). After final PBS washes, cells were mounted, and slides were imaged using an Olympus IX51 microscope (Olympus).

Mitochondrial iron loading

Mitochondrial iron loading and mitochondrial mass were assessed in IM-FEN neurons using MitoFerroGreen (Dojindo, M489) together with MitoTracker Red CMXRos (Thermo Fisher Scientific, M7512). Differentiated IM-FEN cells were treated with vehicle or PA with or without Fer-1, washed with prewarmed HBSS, and incubated with 5 μM MitoFerroGreen and 100 nM MitoTracker Red CMXRos in HBSS for 30 minutes at 37°C in the dark. Cells were then washed, maintained in fresh HBSS, and imaged live by confocal microscopy using appropriate excitation and emission settings for each dye. Regions of interest were drawn around neuronal cell bodies, background was subtracted, and mean fluorescence intensities were quantified using ImageJ/Fiji. Mitochondrial iron loading was expressed as MitoFerroGreen intensity normalized to MitoTracker Red CMXRos signal or to vehicle controls.

Volumetric Analysis of Confocal Z-Stacks from Human Myenteric Ganglia

Volumetric analysis of z-stacks obtained from human networks of myenteric ganglia (nhMPG) was conducted to quantify neuronal viability, ferroptosis marker expression, and nuclear translocation. Confocal images were acquired using a Nikon A1R confocal microscope, with z-stacks spanning ~18 μm in depth at 0.5 μm intervals. See Supplemental Methods for details.

Statistical Analysis

All data are presented as mean ± standard error of the mean (SEM). Statistical analyses were performed using GraphPad Prism version 10.0 (GraphPad Software, San Diego, CA, USA). Depending on the experimental design, comparisons between two groups were conducted using unpaired two-tailed t-tests. Experiments involving more than two groups or more than one factor (e.g., diet, sex, AAV treatment, or PA/Fer-1) were analyzed using one-way or two-way ANOVA models that included the appropriate interaction term. When ANOVA indicated a significant mean or interaction effect, Tukey's post hoc test was used to control type I error across multiple comparisons. A $p< 0.05$ was considered statistically significant and denoted as follows: *$P < 0.05$, **$P < 0.01$, ***$P < 0.001$.

Study approval

All animal procedures were reviewed and approved by the Institutional Animal Care and Use Committee (IACUC) of the Atlanta VA Health Care System, Decatur, Georgia, USA, and were conducted in accordance with NIH guidelines. Human colonic tissues were obtained from patients undergoing elective colectomy under protocols approved by The Ohio State University Institutional Review Board (IRB), Columbus, Ohio, USA (OSU-IRB #2020H0273 and #2024H0125). Written informed consent was obtained from all subjects prior to tissue collection.

Author Contributions

A.B. conceived the project, designed and performed the in vitro and in vivo animal experiments, analyzed data, and wrote the manuscript. D.P. and F.L.C. performed the human nhMPG arm of the study, including tissue procurement, ex vivo treatments, imaging, and

quantitative analysis. Y.D. assisted with human nhMPG isolation, immunofluorescence, and data acquisition. J.R. and A.H. provided surgical samples and clinical metadata. Y.L., F.Ci., and S.M.M. assisted with the design and execution of mouse experiments and molecular assays, and S.M.M. edited the manuscript. P.H. and C.M.H. contributed expertise in ferroptosis mechanisms and data interpretation. W.H. and X.Y. provided guidance on AAV construct design and AAV-based gene delivery experiments. J.M.P. assisted with confocal imaging and image analysis. F.L.C supervised human studies; F.L.C. and D.P. contributed to data interpretation and manuscript submission. S.S. supervised the overall study, secured funding, contributed to experimental design, and edited the manuscript. All authors reviewed and approved the final version of the manuscript. A.B. and D.P. contributed equally to this work. Co-first authorship order was determined by mutual agreement among the co-first authors in consultation with the senior authors, based on overall contribution to study conception, experimentation, analysis, and manuscript preparation.

Funding Support

This work is the result of NIH funding, in part, and is subject to the NIH Public Access Policy. Through acceptance of this federal funding, the NIH has been given a right to make the work publicly available in PubMed Central. This work was supported by the National Institutes of Health (NIH) grant R01 DK080684 (S.S.), RO1 DK125809 (F.L.C), VA Merit Award 2I01BX000136 (S.S), and a mini-sabbatical award from the American Neurogastroenterology and Motility Society (ANMS) awarded (A.B.) to support training in the laboratory of Dr. Fievos L. Christofi at The Ohio State University, focused on the isolation and imaging of human networks of myenteric ganglia.

Acknowledgments

We thank the patients and surgical teams at The Ohio State University Wexner Medical Center for facilitating access to human colonic tissue specimens.

Data Availability

The RNA sequencing dataset generated and analyzed in this study has been deposited in the NCBI Gene Expression Omnibus (GEO) under accession number GSE298679. All other data supporting the findings of this study are available within the article and its supplementary information or from the corresponding author upon reasonable request.

References

1. Furness JB. The enteric nervous system and neurogastroenterology. *Nat Rev Gastroenterol Hepatol.* 2012;9(5):286-94.
2. Gershon MD. The enteric nervous system: a second brain. *Hosp Pract (1995).* 1999;34(7):31-2, 5-8, 41-2 passim.
3. Gershon MD. Review article: roles played by 5-hydroxytryptamine in the physiology of the bowel. *Aliment Pharmacol Ther.* 1999;13 Suppl 2:15-30.
4. Kulkarni S, Micci M-A, Leser J, Shin C, Tang S-C, Fu Y-Y, et al. Adult enteric nervous system in health is maintained by a dynamic balance between neuronal apoptosis and neurogenesis. *Proceedings of the National Academy of Sciences.* 2017;114(18):E3709-E18.
5. Stavely R, Rahman AA, Mueller JL, Leavitt AR, Han CY, Pan W, et al. Mature enteric neurons have the capacity to reinnervate the intestine with glial cells as their guide. *Neuron.* 2024;112(18):3143-60.e6.
6. Eslick GD. Gastrointestinal symptoms and obesity: a meta-analysis. *Obesity Reviews.* 2012;13(5):469-79.
7. Stenkamp-Strahm CM, Kappmeyer AJ, Schmalz JT, Gericke M, and Balemba O. High-fat diet ingestion correlates with neuropathy in the duodenum myenteric plexus of obese mice with symptoms of type 2 diabetes. *Cell Tissue Res.* 2013;354(2):381-94.
8. Shi H, Kokoeva MV, Inouye K, Tzameli I, Yin H, and Flier JS. TLR4 links innate immunity and fatty acid–induced insulin resistance. *J Clin Invest.* 2006;116(11):3015-25.
9. Sivasubramanian MK, Monteiro R, Jagadeesh M, Balasubramanian P, and Subramanian M. Palmitic Acid Induces Oxidative Stress and Senescence in Human Brainstem Astrocytes, Downregulating Glutamate Reuptake Transporters—Implications for Obesity-Related Sympathoexcitation. *Nutrients.* 2024;16(17):2852.
10. Park HR, Kim J-Y, Park K-Y, and Lee J. Lipotoxicity of Palmitic Acid on Neural Progenitor Cells and Hippocampal Neurogenesis. *Toxicological Research.* 2011;27(2):103-10.
11. Stockwell BR, Friedmann Angeli JP, Bayir H, Bush AI, Conrad M, Dixon SJ, et al. Ferroptosis: A Regulated Cell Death Nexus Linking Metabolism, Redox Biology, and Disease. *Cell.* 2017;171(2):273-85.
12. Yang Wan S, SriRamaratnam R, Welsch Matthew E, Shimada K, Skouta R, Viswanathan Vasanthi S, et al. Regulation of Ferroptotic Cancer Cell Death by GPX4. *Cell.* 2014;156(1):317-31.
13. Gao M, Yi J, Zhu J, Minikes AM, Monian P, Thompson CB, and Jiang X. Role of Mitochondria in Ferroptosis. *Mol Cell.* 2019;73(2):354-63.e3.
14. Kenny EM, Fidan E, Yang Q, Anthonymuthu TS, New LA, Meyer EA, et al. Ferroptosis Contributes to Neuronal Death and Functional Outcome After Traumatic Brain Injury. *Crit Care Med.* 2019;47(3):410-8.
15. Abdo H, Derkinderen P, Gomes P, Chevalier J, Aubert P, Masson D, et al. Enteric glial cells protect neurons from oxidative stress in part via reduced glutathione. *Faseb j.* 2010;24(4):1082-94.
16. Itoh K, Wakabayashi N, Katoh Y, Ishii T, Igarashi K, Engel JD, and Yamamoto M. Keap1 represses nuclear activation of antioxidant responsive elements by Nrf2 through binding to the amino-terminal Neh2 domain. *Genes Dev.* 1999;13(1):76-86.
17. Lu XY, Wang HD, Xu JG, Ding K, and Li T. Deletion of Nrf2 Exacerbates Oxidative Stress After Traumatic Brain Injury in Mice. *Cell Mol Neurobiol.* 2015;35(5):713-21.

18. Sun X, Ou Z, Chen R, Niu X, Chen D, Kang R, and Tang D. Activation of the p62-Keap1-NRF2 pathway protects against ferroptosis in hepatocellular carcinoma cells. *Hepatology.* 2016;63(1):173-84.
19. Skouta R, Dixon SJ, Wang J, Dunn DE, Orman M, Shimada K, et al. Ferrostatins Inhibit Oxidative Lipid Damage and Cell Death in Diverse Disease Models. *Journal of the American Chemical Society.* 2014;136(12):4551-6.
20. Ye L, Li G, Goebel A, Raju AV, Kong F, Lv Y, et al. Caspase-11-mediated enteric neuronal pyroptosis underlies Western diet-induced colonic dysmotility. *J Clin Invest.* 2020;130(7):3621-36.
21. Abdelmagid SA, Clarke SE, Nielsen DE, Badawi A, El-Sohemy A, Mutch DM, and Ma DW. Comprehensive profiling of plasma fatty acid concentrations in young healthy Canadian adults. *PLoS One.* 2015;10(2):e0116195.
22. Rojo AI, Innamorato NG, Martín-Moreno AM, De Ceballos ML, Yamamoto M, and Cuadrado A. Nrf2 regulates microglial dynamics and neuroinflammation in experimental Parkinson's disease. *Glia.* 2010;58(5):588-98.
23. Wang R, Zhang J, Ren H, Qi S, Xie L, Xie H, et al. Dysregulated palmitic acid metabolism promotes the formation of renal calcium-oxalate stones through ferroptosis induced by polyunsaturated fatty acids/phosphatidic acid. *Cellular and Molecular Life Sciences.* 2024;81(1):85.
24. Shintoku R, Takigawa Y, Yamada K, Kubota C, Yoshimoto Y, Takeuchi T, et al. Lipoxygenase-mediated generation of lipid peroxides enhances ferroptosis induced by erastin and RSL3. *Cancer Sci.* 2017;108(11):2187-94.
25. Hartl FU, Bracher A, and Hayer-Hartl M. Molecular chaperones in protein folding and proteostasis. *Nature.* 2011;475(7356):324-32.
26. Sun X, Ou Z, Xie M, Kang R, Fan Y, Niu X, et al. HSPB1 as a novel regulator of ferroptotic cancer cell death. *Oncogene.* 2015;34(45):5617-25.
27. Bersuker K, Hendricks JM, Li Z, Magtanong L, Ford B, Tang PH, et al. The CoQ oxidoreductase FSP1 acts parallel to GPX4 to inhibit ferroptosis. *Nature.* 2019;575(7784):688-92.
28. Li D, Lu X, Xu G, Liu S, Gong Z, Lu F, et al. Dihydroorotate dehydrogenase regulates ferroptosis in neurons after spinal cord injury via the P53-ALOX15 signaling pathway. *CNS Neurosci Ther.* 2023;29(7):1923-39.
29. Paradkar PN, Zumbrennen KB, Paw BH, Ward DM, and Kaplan J. Regulation of mitochondrial iron import through differential turnover of mitoferrin 1 and mitoferrin 2. *Mol Cell Biol.* 2009;29(4):1007-16.
30. Dodson M, de la Vega MR, Cholanians AB, Schmidlin CJ, Chapman E, and Zhang DD. Modulating NRF2 in Disease: Timing Is Everything. *Annual Review of Pharmacology and Toxicology.* 2019;59(Volume 59, 2019):555-75.
31. Andrés-Blasco I, Blesa S, Vinué Á, González-Navarro H, Real JT, Martínez-Hervás S, et al. Srebf2 Locus Overexpression Reduces Body Weight, Total Cholesterol and Glucose Levels in Mice Fed with Two Different Diets. *Nutrients.* 2020;12(10).
32. Aranda CJ, Arredondo-Amador M, Ocón B, Lavín JL, Aransay AM, Martínez-Augustin O, and de Medina FS. Intestinal epithelial deletion of the glucocorticoid receptor NR3C1 alters expression of inflammatory mediators and barrier function. *Faseb j.* 2019;33(12):14067-82.

33. Aguilar E, Esteves P, Sancerni T, Lenoir V, Aparicio T, Bouillaud F, et al. UCP2 Deficiency Increases Colon Tumorigenesis by Promoting Lipid Synthesis and Depleting NADPH for Antioxidant Defenses. *Cell Rep.* 2019;28(9):2306-16.e5.
34. Anitha M, Reichardt F, Tabatabavakili S, Nezami BG, Chassaing B, Mwangi S, et al. Intestinal dysbiosis contributes to the delayed gastrointestinal transit in high-fat diet fed mice. *Cell Mol Gastroenterol Hepatol.* 2016;2(3):328-39.
35. Li J, Liu X, Wu Y, Ji W, Tian Q, and Li S. Aerobic exercise improves intestinal mucosal barrier dysfunction through TLR4/MyD88/NF-κB signaling pathway in diabetic rats. *Biochemical and Biophysical Research Communications.* 2022;634:75-82.
36. Clyburn C, Howe CA, Arnold AC, Lang CH, Travagli RA, and Browning KN. Perinatal high-fat diet alters development of GABAA receptor subunits in dorsal motor nucleus of vagus. *American Journal of Physiology-Gastrointestinal and Liver Physiology.* 2019;317(1):G40-G50.
37. Sikander A, Rana SV, Sharma SK, Sinha SK, Arora SK, Prasad KK, and Singh K. Association of alpha 2A adrenergic receptor gene (ADRA2A) polymorphism with irritable bowel syndrome, microscopic and ulcerative colitis. *Clinica Chimica Acta.* 2010;411(1-2):59-63.
38. Sharkey KA, and Wiley JW. The Role of the Endocannabinoid System in the Brain–Gut Axis. *Gastroenterology.* 2016;151(2):252-66.
39. Boules M, Li Z, Smith K, Fredrickson P, and Richelson E. Diverse roles of neurotensin agonists in the central nervous system. *Front Endocrinol (Lausanne).* 2013;4:36.
40. Reichardt F, Chassaing B, Nezami BG, Li G, Tabatabavakili S, Mwangi S, et al. Western diet induces colonic nitrergic myenteric neuropathy and dysmotility in mice via saturated fatty acid- and lipopolysaccharide-induced TLR4 signalling. *J Physiol.* 2017;595(5):1831-46.
41. Gong D, Zhang J, Chen Y, Xu Y, Ma J, Hu G, et al. The m(6)A-suppressed P2RX6 activation promotes renal cancer cells migration and invasion through ATP-induced Ca(2+) influx modulating ERK1/2 phosphorylation and MMP9 signaling pathway. *J Exp Clin Cancer Res.* 2019;38(1):233.
42. Coleman WL, Bill CA, and Bykhovskaia M. Rab3a deletion reduces vesicle docking and transmitter release at the mouse diaphragm synapse. *Neuroscience.* 2007;148(1):1-6.
43. Vardar G, Chang S, Arancillo M, Wu YJ, Trimbuch T, and Rosenmund C. Distinct Functions of Syntaxin-1 in Neuronal Maintenance, Synaptic Vesicle Docking, and Fusion in Mouse Neurons. *J Neurosci.* 2016;36(30):7911-24.
44. Kellner V, Kersbergen CJ, Li S, Babola TA, Saher G, and Bergles DE. Dual metabotropic glutamate receptor signaling enables coordination of astrocyte and neuron activity in developing sensory domains. *Neuron.* 2021;109(16):2545-55.e7.
45. Feng H, Schorpp K, Jin J, Yozwiak CE, Hoffstrom BG, Decker AM, et al. Transferrin Receptor Is a Specific Ferroptosis Marker. *Cell Rep.* 2020;30(10):3411-23.e7.
46. Zhu M, and Yu J. Salidroside alleviates ferroptosis in FAC-induced Age-related macular degeneration models by activating Nrf2/SLC7A11/GPX4 axis. *Int Immunopharmacol.* 2024;142(Pt A):113041.
47. Tuo Qz, Lei P, Jackman KA, Li Xl, Xiong H, Li Xl, et al. Tau-mediated iron export prevents ferroptotic damage after ischemic stroke. *Molecular Psychiatry.* 2017;22(11):1520-30.

48. Do Van B, Gouel F, Jonneaux A, Timmerman K, Gelé P, Pétrault M, et al. Ferroptosis, a newly characterized form of cell death in Parkinson's disease that is regulated by PKC. *Neurobiol Dis.* 2016;94:169-78.
49. Chen K, Tang Y, Lan L, Li M, and Lu Z. Autophagy mediated FTH1 degradation activates gasdermin E dependent pyroptosis contributing to diquat induced kidney injury. *Food and Chemical Toxicology.* 2024;184:114411.
50. Chan JJ, Kwok ZH, Chew XH, Zhang B, Liu C, Soong TW, et al. A FTH1 gene:pseudogene:microRNA network regulates tumorigenesis in prostate cancer. *Nucleic Acids Res.* 2018;46(4):1998-2011.
51. Shieh JT, Tintos-Hernandez JA, Murali CN, Penon-Portmann M, Flores-Mendez M, Santana A, et al. Heterozygous nonsense variants in the ferritin heavy-chain gene FTH1 cause a neuroferritinopathy. *Human Genetics and Genomics Advances.* 2023;4(4).
52. Linan-Rico A, Ochoa-Cortes F, Schneider R, and Christofi FL. Mini-review: Enteric glial cell reactions to inflammation and potential therapeutic implications for GI diseases, motility disorders, and abdominal pain. *Neuroscience Letters.* 2023;812:137395.
53. Liang P, Zhang X, Zhang Y, Wu Y, Song Y, Wang X, et al. Neurotoxic A1 astrocytes promote neuronal ferroptosis via CXCL10/CXCR3 axis in epilepsy. *Free Radic Biol Med.* 2023;195:329-42.
54. Escartin C, Galea E, Lakatos A, O'Callaghan JP, Petzold GC, Serrano-Pozo A, et al. Reactive astrocyte nomenclature, definitions, and future directions. *Nature Neuroscience.* 2021;24(3):312-25.
55. Ishii T, Warabi E, and Mann GE. Circadian control of BDNF-mediated Nrf2 activation in astrocytes protects dopaminergic neurons from ferroptosis. *Free Radic Biol Med.* 2019;133:169-78.
56. Murray MB, and Dixon SJ. Ferroptosis regulation by Cap'n'collar family transcription factors. *Journal of Biological Chemistry.* 2024;300(8):107583.
57. Anitha M, Joseph I, Ding X, Torre ER, Sawchuk MA, Mwangi S, et al. Characterization of Fetal and Postnatal Enteric Neuronal Cell Lines With Improvement in Intestinal Neural Function. *Gastroenterology.* 2008;134(5):1424-35.
58. Mazzotta E, Grants I, Villalobos-Hernandez E, Chaudhuri S, McClain JL, Seguella L, et al. BQ788 reveals glial ETB receptor modulation of neuronal cholinergic and nitrergic pathways to inhibit intestinal motility: Linked to postoperative ileus. *British Journal of Pharmacology.* 2023;180(19):2550-76.
59. Liñán-Rico A, Turco F, Ochoa-Cortes F, Harzman A, Needleman BJ, Arsenescu R, et al. Molecular Signaling and Dysfunction of the Human Reactive Enteric Glial Cell Phenotype: Implications for GI Infection, IBD, POI, Neurological, Motility, and GI Disorders. *Inflamm Bowel Dis.* 2016;22(8):1812-34.
60. Grundmann D, Klotz M, Rabe H, Glanemann M, and Schäfer KH. Isolation of high-purity myenteric plexus from adult human and mouse gastrointestinal tract. *Sci Rep.* 2015;5:9226.
61. Villalobos-Hernandez EC, Ochoa-Cortes F, Mazzotta E, Chaudhuri S, Soghomonyan S, Diaz JF, et al. 212: ROUTINE PATCH-CLAMP RECORDINGS IN ISOLATED INTACT NEURAL NETWORKS OF HUMAN MYENTERIC GANGLIA IS A SUITABLE AND RELIABLE IN VITRO TECHNIQUE TO STUDY THE “HUMAN LITTLE BRAIN IN THE GUT&#x201d. *Gastroenterology.* 2022;162(7):S-37.

Figure legends

Figure 1. PA induces ferroptosis-associated iron accumulation in enteric neuronal cells. IM-FEN and primary enteric neurons were treated with Veh, PA, 0.5 mM, Fer-1, 10 μM, or PA + Fer-1 for 24h to assess ferroptosis-related iron dysregulation. (A) Heatmap of RNA-seq data showing differential expression of ferroptosis- and iron-regulatory genes in enteric neuron cell lines treated with Veh or PA. (B) qRT-PCR analysis of TfR1, DMT1, GPX4, IL6, and SLC40A1 mRNA levels in enteric neuron cell lines treated with Veh or PA, normalized to Hprt1. (C-D) Western blot analysis of FTH1 protein levels in IM-FEN treated with Veh, PA, Fer-1, or PA + Fer-1; β-actin serves as loading control. (E) Immunofluorescence staining of TUBB3 (green) and FTH1 (red) in primary enteric neurons treated with Veh, PA, or PA+Fer-1. (F) Immunofluorescence staining of TUBB3 (green) and TfR1 (red) in primary enteric neurons treated as in (E), showing PA-induced TfR1 upregulation reversed by Fer-1. (G) FeRhoNox-1 staining of labile Fe^{2+} (red) with DAPI (blue) in primary enteric neurons treated as in (E), showing PA-induced iron accumulation blocked by Fer-1. Histograms represent fold change in signal intensity relative to Veh. Scale bars: 50 μm. Data represents three independent experiments. Statistics: (B-C) unpaired, 2-tailed t test; (D-G) 1-way ANOVA with Tukey's multiple-comparisons test. *P< 0.05, **P< 0.01, ***P<0.001; ns, not significant.

Figure 2. PA Triggers Ferroptotic Stress and Loss of Enteric Neuronal Identity via Lipid Peroxidation. IM-FEN and primary enteric neurons were treated with Veh, PA, 0.5 mM, Fer-1, 10 μM, or PA+Fer-1 for 24h to assess ferroptosis-associated cell death, lipid peroxidation, and neuronal identity loss. (A-B) Heatmaps of RNA-seq data showing differential expression of neuronal and associated cellular markers (A), and inflammatory and stress-response markers (B), in enteric neurons treated with Veh or PA. (C) Representative images of enteric neurons stained with propidium iodide (PI, magenta) and DAPI (blue). Histograms show quantification of PI^+ nuclei (cell death) and total viable cell counts, indicating PA-induced cytotoxicity reversed by Fer-1. (D) qRT-PCR analysis of nNOS and TUBB3 mRNA expression in primary enteric neurons treated as in (C), normalized to 18s rRNA. (E-G) Primary enteric neurons were treated as described above. (E) Immunofluorescence staining for TUBB3 (cyan) and ALOX15 (magenta). (F) Immunofluorescence staining for TUBB3 (green) and GPX4 (red), showing loss of GPX4 with PA rescued by Fer-1. (G) Immunofluorescence staining for TUBB3 (cyan) and 4-HNE (red), showing PA-induced lipid peroxidation reversed by Fer-1. Histograms represent fold change in fluorescence intensity relative to Veh. Scale bars: 50 μm. Data represents three independent experiments. Statistics: (C-G) 1-way ANOVA with Tukey's multiple-comparisons test; (D) 1-way ANOVA with Tukey's multiple-comparisons test. *P < 0.05, **P < 0.01, ***P < 0.001; ns, not significant.

Figure 3. PA drives mitochondrial ferroptosis via ROS accumulation, mitochondrial disruption, and MFRN2 upregulation. IM-FEN and primary enteric neurons were treated with Veh, PA, 0.5 mM, Fer-1, 10 μM, or PA+Fer-1 for 24h to examine mitochondrial oxidative stress and ferroptosis-related mitochondrial changes. (A) Heatmap of mitochondrial dysfunction and ferroptosis-related markers in enteric neurons treated with Veh or PA. (B) Heatmap of mitochondrial Complex I-associated regulators of ferroptosis in the same conditions. (C) MitoFerroGreen (green) and MitoTracker Red (red) staining in IM-FEN cells showing increased mitochondria-associated labile iron (Fe^{2+}) after PA treatment, which is partially reduced by co-treatment with Fer-1; histogram shows fold change in MitoFerroGreen fluorescence colocalized with MitoTracker relative to Veh. (D) Immunofluorescence staining of primary enteric neurons for TUBB3 (cyan) and MitoBrilliant 646 (magenta), with magnified insets, showing PA-induced mitochondrial disruption, rescued by Fer-1. (E) Immunofluorescence staining of primary enteric neurons for TUBB3 (green) and MFRN2 (brown), showing increased MFRN2 expression with PA, reversed by Fer-1. Histograms represent fold change in fluorescence intensity relative to Veh.

Scale bars: 50 μm. Data represents three independent experiments. Statistics: (C-E) one-way ANOVA with Tukey's multiple-comparisons test. *P< 0.05, **P< 0.01, ***P< 0.001; ns, not significant.

Figure 4. Ferroptotic injury in response to chronic but not acute exposure of 0.5mM PA is sensitive to the ferroptosis inhibitor (Fer-1) in IM-FEN enteric neurons. (A) Chronic PA exposure abolishes Ca^{2+} responses in IM-FEN in response to EFS. A representative example of a frequency-dependent EFS Ca^{2+}response is shown in IM-FEN; cells were loaded with the fluo-4 Ca^{2+} indicator. The Ca^{2+}transients are shown in the panel on the right for the various treatments. PA abolished responses and pretreatment with Fer-1 preserved Ca^{2+} signaling. TTX eliminated all EFS activity. (B) Identical frequency-response Ca^{2+}curves were obtained in mouse IM-FEN neurons and neurons in LMMP mouse preparations in Wnt1:GCaMP Ca^{2+}reporter mice. (C) Pooled data show that chronic exposure (24h) to 0.5mM PA abolishes the EFS-response in IM-FEN neurons. Fer-1 prevents the chronic effect of PA. EFS responses are blocked by TTX and therefore involve neuronal Na_v channels and nerve conduction. (D) Acute PA exposure leads to direct concentration-dependent increases in neuronal Ca^{2+}response from 0.01-0.5mM. Responses are not sensitive to Fer-1. (E) Acute PA exposure (0.01-0.5mM) does not cause significant neuronal cell death, whereas chronic PA exposure (0.5mM) causes significant cell death in the IM-FEN population; PI exclusion assay. (F) Differential effects of acute exposure to different concentrations of PA on neuronal activity. PA 0.1mM reduced Ca^{2+}responses. PA 0.5 mM augments EFS responses at lower frequencies of stimulation and the responses are only partially TTX-sensitive. (G) Pooled data for acute PA effects show that PA 0.1mM was sufficient to nearly abolish EFS responses, whereas PA 0.5mM enhances responses at low-to-intermediate frequencies, does not block the EFS response and is associated with a TTX-insensitive component; EFS responses are normally abolished by TTX. (H) Fer-1 had no effect on frequency-dependent responses during acute PA exposure (pooled data). Two-way ANOVA was used for statistical comparisons between curves. *P<0.05, **P<0.01, ***P<0.001; ns, not significant.

Figure 5. PA suppresses phospho-Nfe2l2 in enteric neurons, while AAV-mediated Nfe2l2 overexpression restores redox signaling *In Vivo*. To assess the effect of palmitate on Nfe2l2 signaling and the therapeutic potential of AAV-mediated Nfe2l2 overexpression, we performed *in vitro* and *in vivo* analyses in enteric neurons and colon tissues. (A) Immunofluorescence staining of primary enteric neurons for TUBB3 (green) and phospho-Nfe2l2 (orange), showing reduced phospho-Nfe2l2 expression with PA treatment (0.5 mM, 24h), rescued by Fer-1 (10 μM). Data represents three independent experiments. (B) Experimental timeline for in vivo study: male and female mice were fed control diet (CD) or Western diet (WD) for 12 weeks, received retro-orbital AAV-eGFP or AAV-Nfe2l2 at week 2, and were phenotyped at week 11 before tissue collection. (C) Immunofluorescence staining of colon sections from CD-fed male and female mice treated with AAV-eGFP or AAV-Nfe2l2, co-stained for TUBB3 (cyan) and total Nfe2l2 (t-Nfe2l2, red). Merged images show enhanced neuronal Nfe2l2 expression in AAV-Nfe2l2-treated mice. Histogram shows fold change in t-Nfe2l2 fluorescence intensity within $TUBB3^+$ neurons. (D-E) Gastrointestinal motility measured by bead expulsion time in Male and Female. n=4 mice for AAV-eGFP groups, n=3 mice for AAV-Nfe2l2 groups. Scale bars: 50 μm. Quantification histograms represent fold change relative to vehicle or AAV-eGFP group as appropriate. Statistics: (A) one-way ANOVA with Tukey's multiple-comparisons test. (C) unpaired two-tailed t test. (D-E) two-way ANOVA with Tukey's multiple-comparisons test. *P < 0.05; **P < 0.01; ***P < 0.001; ns, not significant.

Figure 6. Western diet increases transferrin receptor and ferritin levels in myenteric ganglia, mitigated by Nfe2l2 overexpression. (A) Immunofluorescence staining of colonic myenteric ganglia for TUBB3 (cyan) and transferrin receptor 1 (TfR1, red) in CD and WD mice treated with AAV-eGFP or AAV-Nfe2l2. Histogram shows fold change in TfR1 fluorescence intensity relative to CD AAV-eGFP (Veh). (B) Immunofluorescence staining for TUBB3 (cyan) and ferritin heavy chain (FTH-1, red) in the same groups. Histogram shows fold change in FTH-1 fluorescence intensity relative to CD AAV-eGFP (Veh). A total of 28 mice were analyzed: n = 4 per group for CD and WD AAV-eGFP, and n = 3 per group for CD and WD AAV-Nfe2l2. For each mouse, 6-10 randomly selected myenteric ganglia were imaged and quantified. Scale bars: 50 μm. Statistics: two-way ANOVA with Tukey's multiple-comparisons test. *P< 0.05; **P< 0.01; ***P< 0.001; ns, not significant.

Figure 7. PA increased cell death in isolated networks of human myenteric ganglia from colectomy surgical specimens. Networks of human myenteric ganglia (nhMPG) were isolated from colectomy surgical specimens and treated with PA or vehicle (DMEM) ex vivo. (A-B) PA (0.5mM) increased PI fluorescence in HuC/D+ nuclei/field (counter stained with DAPI) compared to DMEM in nhMPG. (C-E) PA shows a significant increase in PI+ neurons/field, increase in PI intensity in neurons/field, and increase in PI+ area co-localized in each neuron. (F) PA increased nuclear translocation of HuC/D protein, a sign of stress on the neurons. Neuronal translocation was analyzed by colocalization of HuC/D+ immunoreactivity and DAPI in nuclei. (G) PA also decreased the density of neurons as well as intensity of HuC/D immunoreactivity (H) in neurons. (I) Cross-sections of z-stack images are used to further illustrate the effect of PA on increasing neuronal cell death and nuclear translocation of HuC/D. NIS Elements co-localization software was used to quantify cell death, translocation, TfR1 activation and FTH-1 activation in 18μm thick confocal z-stacks captured at 0.5μm optical sections; n=36 different networks analyzed for each treatment. Data was analyzed from gut surgical specimens procured from 3 human subjects for each parameter; 12 Z-stacks in different networks of ganglia (nhMPG networks) in each patient were used for colocalization analysis and statistics. Statistics: one-way ANOVA with Tukey's multiple-comparisons test. Data means SEM. *P < 0.05; **P< 0.01; ***P< 0.001; ns, not significant. Scale bars: 50 μm (A and B); 10 μm (I).

Figure 8. PA induction of Transferrin Receptor-1 (TfR1) expression in human myenteric neurons of nhMPG networks. Networks of human myenteric ganglia (nhMPG) isolated from surgical specimens were treated ex vivo with PA, DMEM, or vehicle control to assess neuronal TfR1 expression. (A-E) PA increased TfR1 expression in HuC/D+ neurons of hMPG networks, compared to DMEM or vehicle control. (E) Images shown are cross-sections of z-stack images through the networks of ganglia, to further illustrate neuronal TfR1. (F-H) PA caused an increase in the number of neurons/fields that expressed TfR1, the area of co-localization of TfR1 and HuC/D+ neurons/field, and it increased TfR1 expression (pixel intensity/field). Statistics: one-way ANOVA with Tukey's multiple-comparisons test. Data means SEM. *P< 0.05; **P< 0.01; ***P< 0.001; ns, not significant.

Figure 9. PA induction of FTH-1 expression in human myenteric neurons of nhMPG networks. nhMPG networks are exposed to DMEM, Vehicle or Palmitate for 24h and stained for FTH-1 (A-D). Pooled data are summarized in (E-G) showing significant upregulation of FTH-1 in neurons with an increase in numbers of HuC/D+ neurons expressing FTH-1, an increase in expression /neuron (intensity), and an associated increase in area of co-localization of FTH-1 with HuC/D+ neurons. (H-J) Secondary analysis showed that non-neuronal FTH-1 levels were also significantly elevated in nhMPG networks, suggesting that FTH-1 upregulation is not restricted to

enteric neurons in response to PA. Statistics: one-way ANOVA with Tukey's multiple-comparisons test. Data mean ± SEM. *P < 0.05; **P < 0.01; ***P < 0.001; ns, not significant.

Figure 10. PA induces ferroptotic enteric neurodegeneration through iron accumulation, oxidative stress, and mitochondrial dysfunction in murine and human models. Schematic summary of the proposed mechanism by which chronic palmitic acid (PA), a major dietary saturated fatty acid, drives ferroptotic injury in enteric neurons, integrating findings from murine models and human networks of myenteric ganglia (nhMPG). Numbered steps: (**1**) Chronic PA exposure. (**2**) Increased iron uptake and trafficking through upregulation of transferrin receptor 1 (TfR1), divalent metal transporter 1 (DMT1), and ZIP14, expanding the intracellular labile Fe^{2+} pool and promoting iron retention. (**3**) Impaired antioxidant defense via suppression of cystine transport and the glutathione (GSH)-GPX4 axis, further sensitizing neurons to oxidative injury. (**4**) Functional ENS impairment, shown as suppressed neuronal activity and excitability (blunted intracellular free calcium $[Ca^{2+}]i$ response to electrical stimulation). (**5**) Convergent iron-driven oxidative stress and lipid peroxidation culminate in enteric neuronal ferroptosis and cell death, leading to neuronal loss and motility dysfunction. Fer-1 inhibits lipid peroxidation and preserves neuronal activity and excitability, mitigating ferroptotic cell death. Created with BioRender (2025).

Figure-1

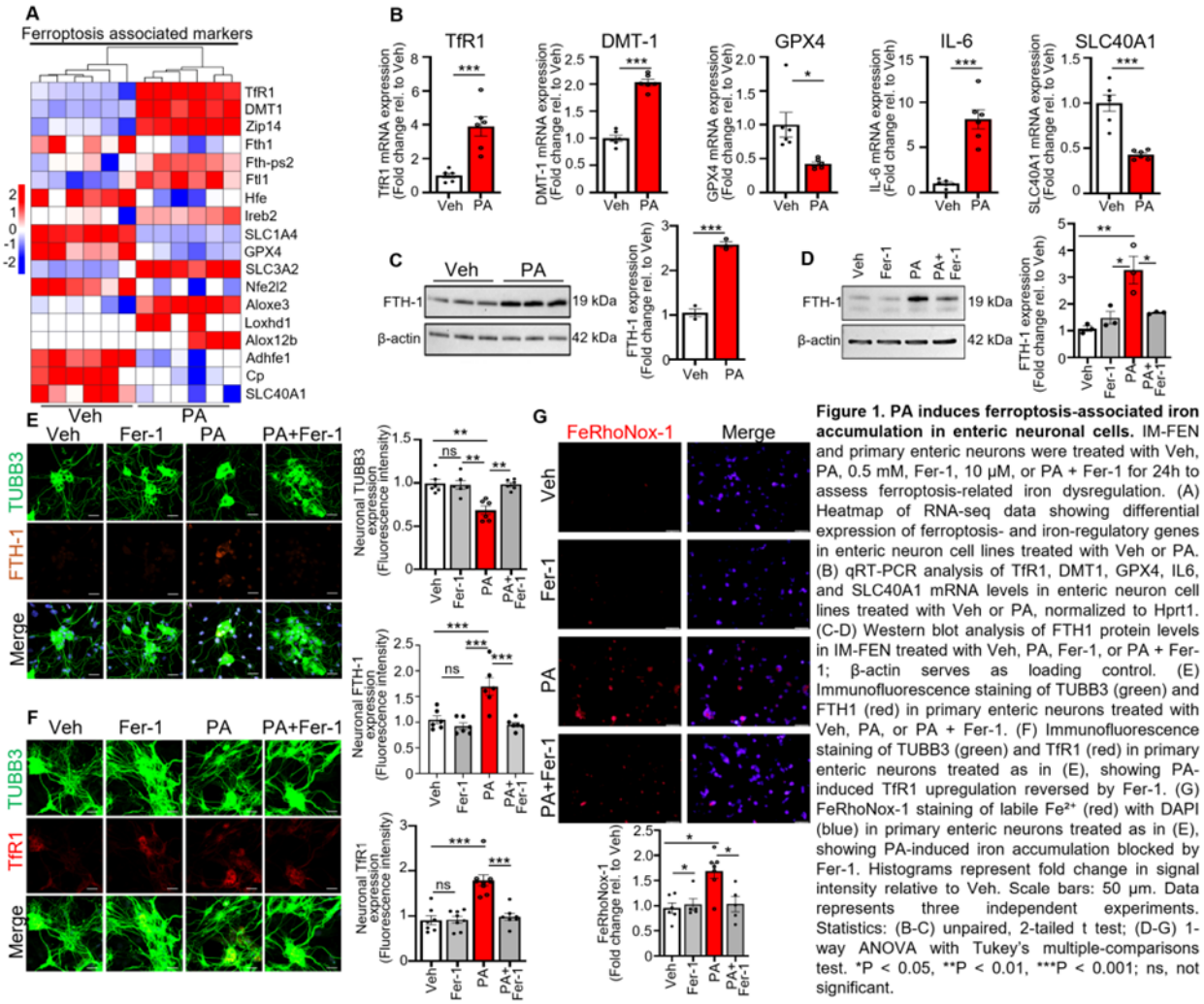

Figure 1. PA induces ferroptosis-associated iron accumulation in enteric neuronal cells. IM-FEN and primary enteric neurons were treated with Veh, PA, 0.5 mM, Fer-1, 10 μM, or PA + Fer-1 for 24h to assess ferroptosis-related iron dysregulation. (A) Heatmap of RNA-seq data showing differential expression of ferroptosis- and iron-regulatory genes in enteric neuron cell lines treated with Veh or PA. (B) qRT-PCR analysis of TfR1, DMT1, GPX4, IL6, and SLC40A1 mRNA levels in enteric neuron cell lines treated with Veh or PA, normalized to Hprt1. (C-D) Western blot analysis of FTH1 protein levels in IM-FEN treated with Veh, PA, Fer-1, or PA + Fer-1; β-actin serves as loading control. (E) Immunofluorescence staining of TUBB3 (green) and FTH1 (red) in primary enteric neurons treated with Veh, PA, or PA + Fer-1. (F) Immunofluorescence staining of TUBB3 (green) and TfR1 (red) in primary enteric neurons treated as in (E), showing PA-induced TfR1 upregulation reversed by Fer-1. (G) FeRhoNox-1 staining of labile Fe^{2+} (red) with DAPI (blue) in primary enteric neurons treated as in (E), showing PA-induced iron accumulation blocked by Fer-1. Histograms represent fold change in signal intensity relative to Veh. Scale bars: 50 μm. Data represents three independent experiments. Statistics: (B-C) unpaired, 2-tailed t test; (D-G) 1-way ANOVA with Tukey's multiple-comparisons test. *P < 0.05, **P < 0.01, ***P < 0.001; ns, not significant.

Figure-2

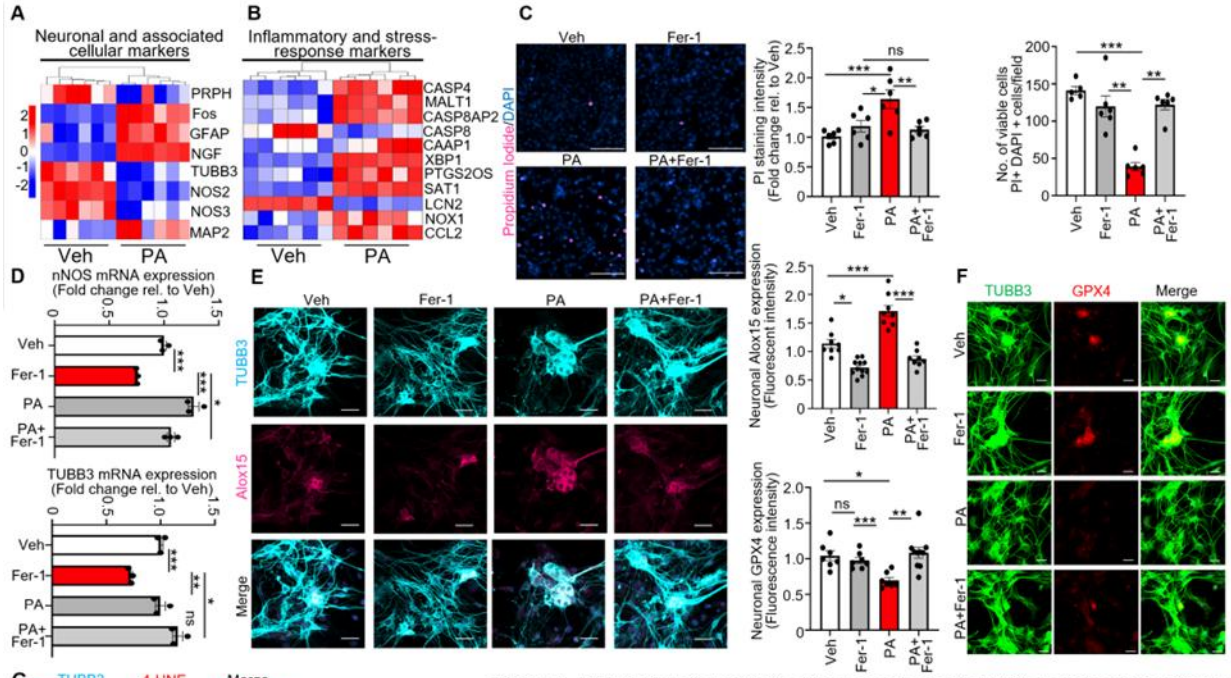

Figure 2. PA triggers ferroptotic stress and loss of enteric neuronal identity via lipid peroxidation. IM-FEN and primary enteric neurons were treated with Veh, PA, 0.5 mM, Fer-1, 10 μM, or PA+Fer-1 for 24h to assess ferroptosis-associated cell death, lipid peroxidation, and neuronal identity loss. (A-B) Heatmaps of RNA-seq data showing differential expression of neuronal and associated cellular markers (A), and inflammatory and stress-response markers (B), in enteric neurons treated with Veh or PA. (C) Representative images of enteric neurons stained with propidium iodide (PI, magenta) and DAPI (blue). Histograms show quantification of PI^+ nuclei (cell death) and total viable cell counts, indicating PA-induced cytotoxicity reversed by Fer-1. (D) qRT-PCR analysis of nNOS and TUBB3 mRNA expression in primary enteric neurons treated as in (C), normalized to 18s rRNA. (E-G) Primary enteric neurons were treated as described above. (E) Immunofluorescence staining for TUBB3 (cyan) and ALOX15 (magenta). (F) Immunofluorescence staining for TUBB3 (green) and GPX4 (red), showing loss of GPX4 with PA rescued by Fer-1. (G) Immunofluorescence staining for TUBB3 (cyan) and 4-HNE (red), showing PA-induced lipid peroxidation reversed by Fer-1. Histograms represent fold change in fluorescence intensity relative to Veh. Scale bars: 50 μm. Data represents three independent experiments. Statistics: (C-G) 1-way ANOVA with Tukey's multiple-comparisons test; (D) 1-way ANOVA with Tukey's multiple-comparisons test. *P < 0.05, **P < 0.01, ***P < 0.001; ns, not significant.

Figure-3

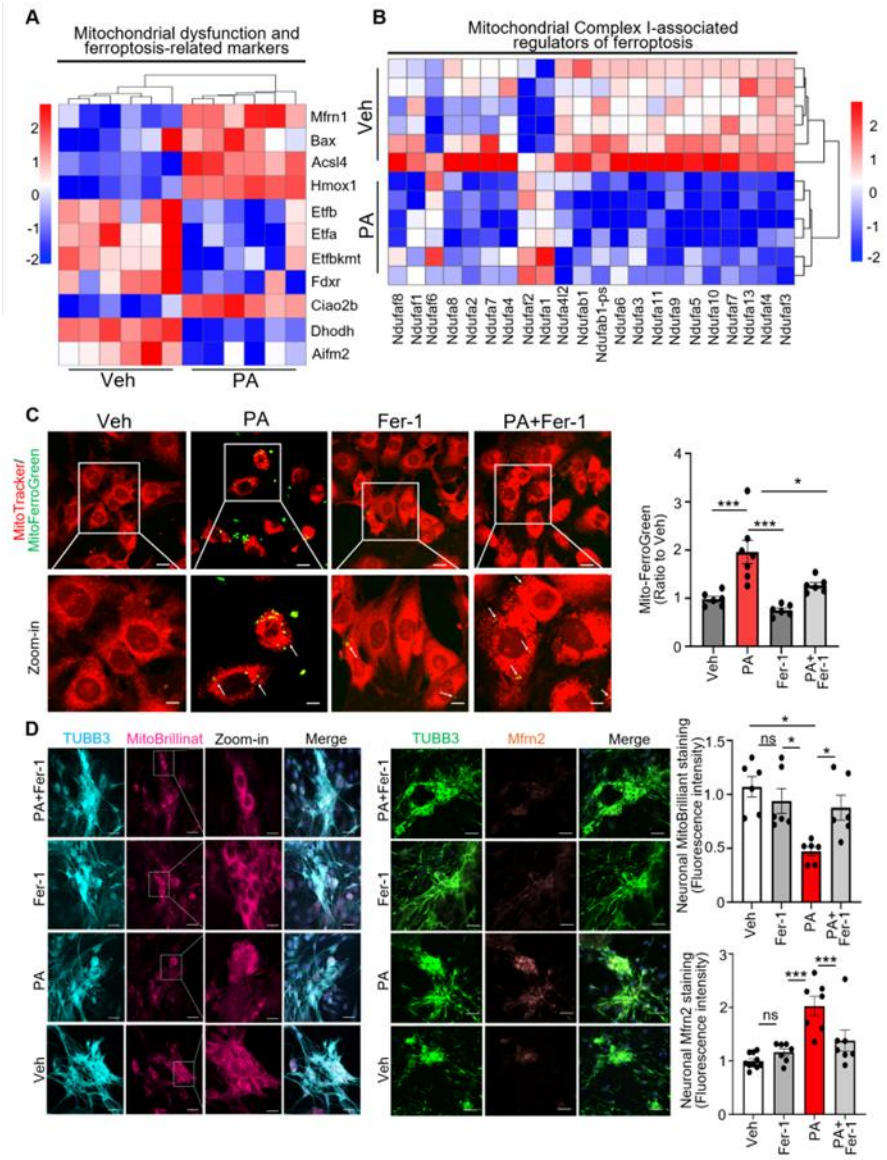

Figure 3. PA drives mitochondrial ferroptosis via ROS accumulation, mitochondrial disruption, and MFRN2 upregulation. IM-FEN and primary enteric neurons were treated with Veh, PA, 0.5 mM, Fer-1, 10 μM, or PA + Fer-1 for 24h to examine mitochondrial oxidative stress and ferroptosis-related mitochondrial changes. (A) Heatmap of mitochondrial dysfunction and ferroptosis-related markers in enteric neurons treated with Veh or PA. (B) Heatmap of mitochondrial Complex I-associated regulators of ferroptosis in the same conditions. (C) MitoFerroGreen (green) and MitoTracker Red (red) staining in IM-FEN cells showing increased mitochondria-associated labile iron (Fe^{2+}) after PA treatment, which is partially reduced by co-treatment with Fer-1; histogram shows fold change in MitoFerroGreen fluorescence colocalized with MitoTracker relative to Veh. (D) Immunofluorescence staining of primary enteric neurons for TUBB3 (cyan) and MitoBrilliant (magenta), with magnified insets, showing PA-induced mitochondrial disruption, rescued by Fer-1. Immunofluorescence staining of primary enteric neurons for TUBB3 (green) and MFRN2 (brown), showing increased MFRN2 expression with PA, reversed by Fer-1. Histograms represent fold change in fluorescence intensity relative to Veh. Scale bars: 50 μm. Data represents three independent experiments. Statistics: (C-E) one-way ANOVA with Tukey's multiple-comparisons test. *P < 0.05, **P < 0.01, ***P < 0.001; ns, not significant.

Figure-4

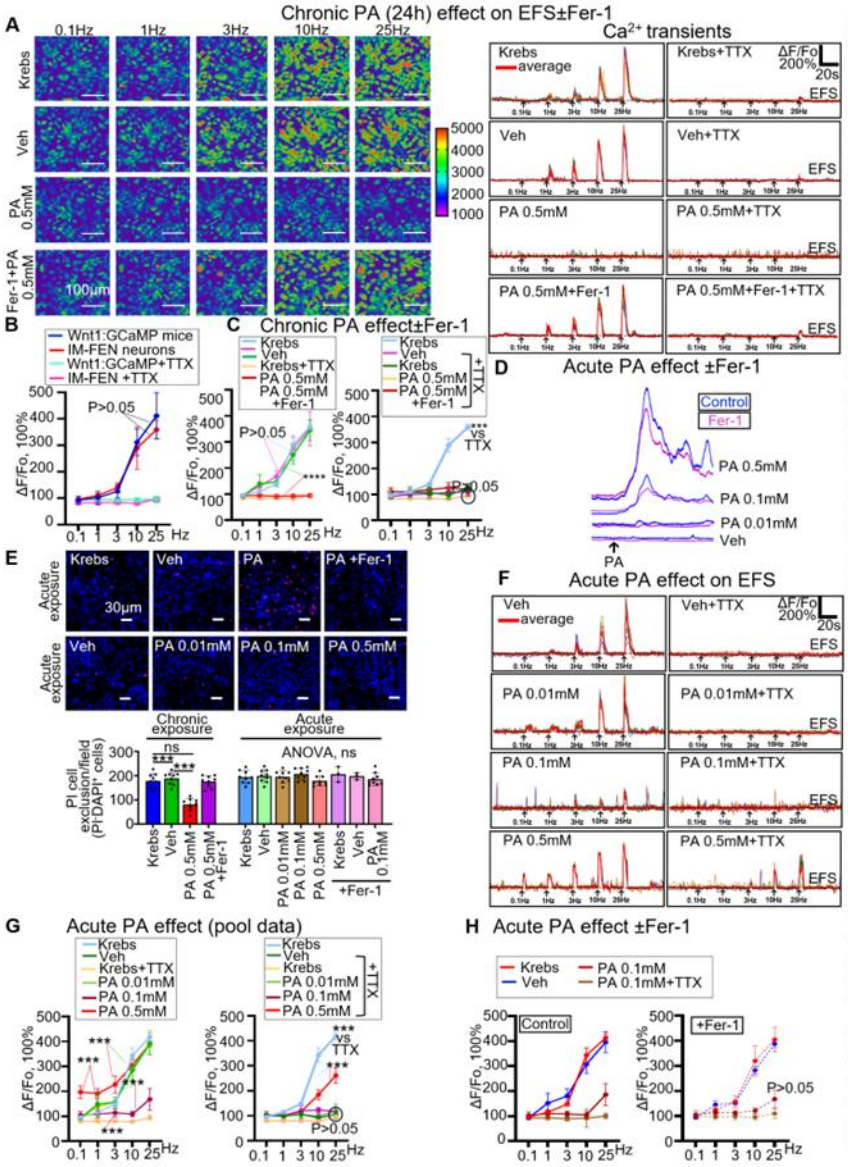

Figure 4. Ferroptotic injury in response to chronic but not acute exposure of 0.5mM PA is sensitive to the ferroptosis inhibitor (Fer-1) in IM-FEN enteric neurons.

(A) Chronic PA exposure abolishes Ca^{2+} responses in IM-FEN in response to EFS. A representative example of a frequency-dependent EFS Ca^{2+}response is shown in IM-FEN; cells were loaded with the fluo-4 Ca^{2+} indicator. The Ca^{2+}transients are shown in the panel on the right for the various treatments. PA abolished responses and pretreatment with Fer-1 preserved Ca^{2+} signaling. TTX eliminated all EFS activity. (B) Identical frequency-response Ca^{2+}curves were obtained in mouse IM-FEN neurons and neurons in LMMP mouse preparations in Wnt1:GCaMP Ca^{2+}reporter mice. (C) Pooled data show that chronic exposure (24h) to 0.5mM PA abolishes the EFS-response in IM-FEN neurons. Fer-1 prevents the chronic effect of PA. EFS responses are blocked by TTX and therefore involve neuronal Na_v channels and nerve conduction. (D) Acute PA exposure leads to direct concentration-dependent increases in neuronal Ca^{2+}response from 0.01-0.5mM. Responses are not sensitive to Fer-1. (E) Acute PA exposure (0.01-0.5mM) does not cause significant neuronal cell death, whereas chronic PA exposure (0.5mM) causes significant cell death in the IM-FEN population; PI exclusion assay. (F) Differential effects of acute exposure to different concentrations of PA on neuronal activity. PA 0.1mM reduced Ca^{2+}responses. PA 0.5 mM augments EFS responses at lower frequencies of stimulation and the responses are only partially TTX-sensitive. (G) Pooled data for acute PA effects show that PA 0.1mM was sufficient to nearly abolish EFS responses, whereas PA 0.5mM enhances responses at low-to-intermediate frequencies, does not block the EFS response and is associated with a TTX-insensitive component; EFS responses are normally abolished by TTX. (H) Fer-1 had no effect on frequency-dependent responses during acute PA exposure (pooled data). Two-way ANOVA was used for statistical comparisons between curves. *P<0.05, **P<0.01, ***P<0.001; ns, not significant.

Figure-5

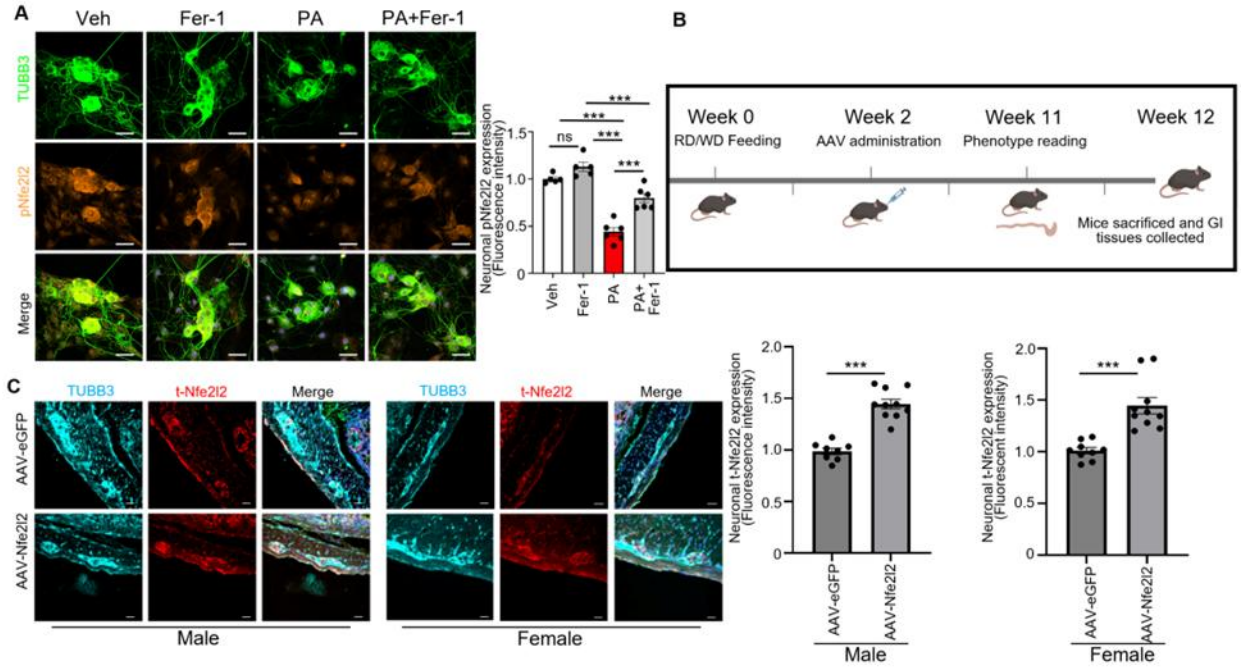

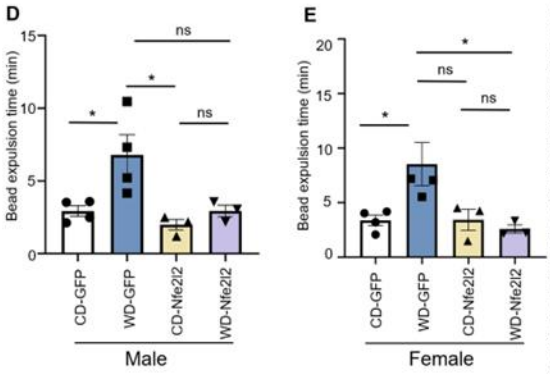

Figure 5. PA suppresses phospho-Nfe2l2 in enteric neurons, while AAV-mediated Nfe2l2 overexpression restores redox signaling *In Vivo*. To assess the effect of palmitate on Nfe2l2 signaling and the therapeutic potential of AAV-mediated Nfe2l2 overexpression, we performed *in vitro* and *in vivo* analyses in enteric neurons and colon tissues. (A) Immunofluorescence staining of primary enteric neurons for TUBB3 (green) and phospho-Nfe2l2 (orange), showing reduced phospho-Nfe2l2 expression with PA treatment (0.5 mM, 24h), rescued by Fer-1 (10 μM). Data represents three independent experiments. (B) Experimental timeline for in vivo study: male and female mice were fed control diet (CD) or Western diet (WD) for 12 weeks, received retro-orbital AAV-eGFP or AAV-Nfe2l2 at week 2, and were phenotyped at week 11 before tissue collection. (C) Immunofluorescence staining of colon sections from CD-fed male and female mice treated with AAV-eGFP or AAV-Nfe2l2, co-stained for TUBB3 (cyan) and total Nfe2l2 (t-Nfe2l2, red). Merged images show enhanced neuronal Nfe2l2 expression in AAV-Nfe2l2-treated mice. Histogram shows fold change in t-Nfe2l2 fluorescence intensity within TUBB3$^+$ neurons. (D-E) Gastrointestinal motility measured by bead expulsion time in Male and Female. n = 4 mice for AAV-eGFP groups, n = 3 mice for AAV-Nfe2l2 groups. Scale bars: 50 μm. Quantification histograms represent fold change relative to vehicle or AAV-eGFP group as appropriate. Statistics: (A) one-way ANOVA with Tukey's multiple-comparisons test. (C) unpaired two-tailed t test. (D-E) two-way ANOVA with Tukey's multiple-comparisons test. *P < 0.05; **P < 0.01; ***P < 0.001; ns, not significant.

Figure-6

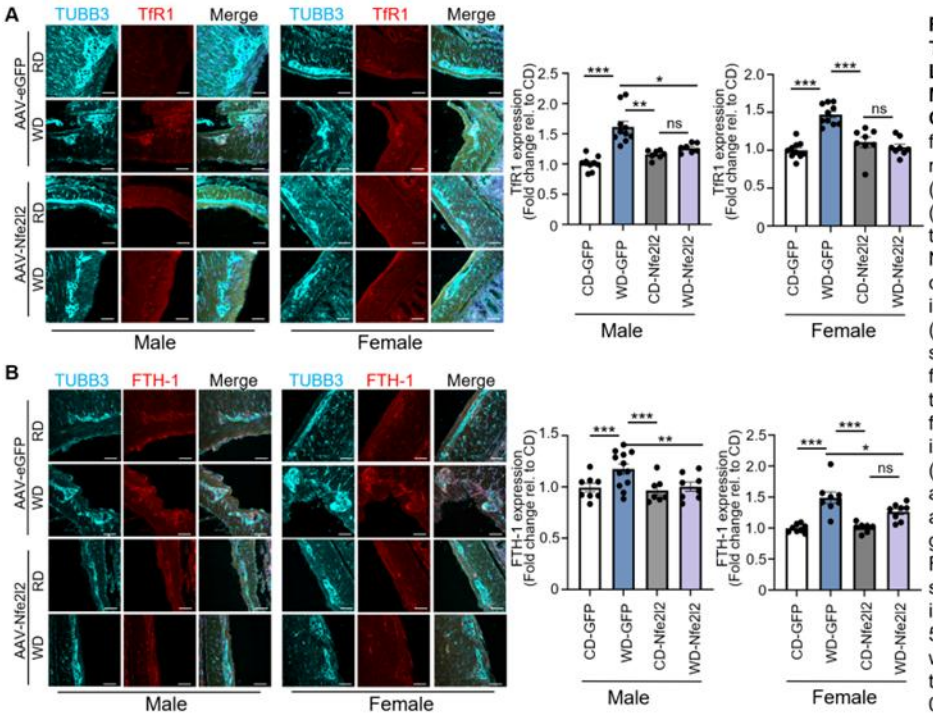

Figure 6. Western Diet Increases Transferrin Receptor and Ferritin Levels in Myenteric Ganglia, Mitigated by Nfe2l2 Overexpression. (A) Immunofluorescence staining of colonic myenteric ganglia for TUBB3 (cyan) and transferrin receptor 1 (TfR1, red) in CD and WD mice treated with AAV-eGFP or AAV-Nfe2l2. Histogram shows fold change in TfR1 fluorescence intensity relative to CD AAV-eGFP (Veh). (B) Immunofluorescence staining for TUBB3 (cyan) and ferritin heavy chain (FTH-1, red) in the same groups. Histogram shows fold change in FTH-1 fluorescence intensity relative to CD AAV-eGFP (Veh). A total of 28 mice were analyzed: n = 4 per group for CD and WD AAV-eGFP, and n = 3 per group for CD and WD AAV-Nfe2l2. For each mouse, 6-10 randomly selected myenteric ganglia were imaged and quantified. Scale bars: 50 µm. Statistics: two-way ANOVA with Tukey's multiple-comparisons test. *P < 0.05; **P < 0.01; ***P < 0.001; ns, not significant.

Figure-7

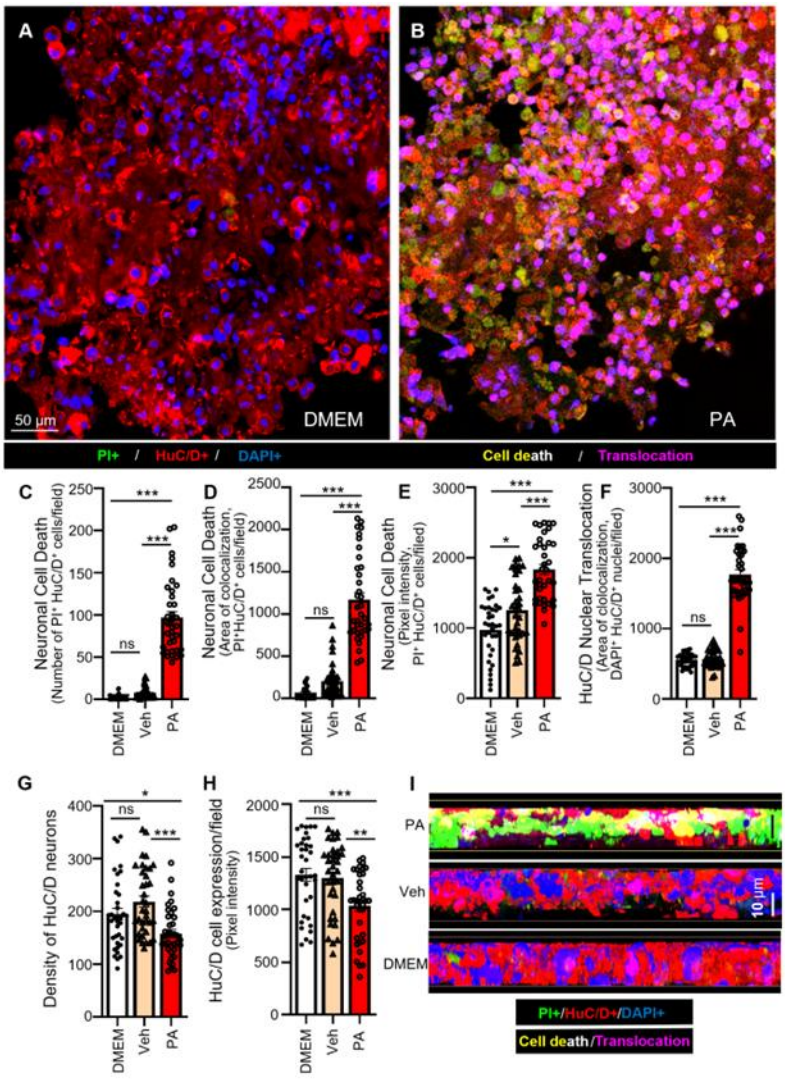

Figure 7. PA increased cell death in isolated networks of human myenteric ganglia from colectomy surgical specimens. Networks of human myenteric ganglia (nhMPG) were isolated from colectomy surgical specimens and treated with PA or vehicle (DMEM) ex vivo. (A-B) PA (0.5mM) increased PI fluorescence in HuC/D+ nuclei/field (counter stained with DAPI) compared to DMEM in nhMPG. (C-E) PA shows a significant increase in PI+ neurons/field, increase in PI intensity in neurons/field, and increase in PI+ area co-localized in each neuron. (F) PA increased nuclear translocation of HuC/D protein, a sign of stress on the neurons. Neuronal translocation was analyzed by colocalization of HuC/D+ immunoreactivity and DAPI in nuclei. (G) PA also decreased the density of neurons as well as intensity of HuC/D immunoreactivity (H) in neurons. (I) Cross-sections of z-stack images are used to further illustrate the effect of PA on increasing neuronal cell death and nuclear translocation of HuC/D. NIS Elements co-localization software was used to quantify cell death, translocation, TfR1 activation and FTH-1 activation in 18µm thick confocal z-stacks captured at 0.5µm optical sections; n=36 different networks analyzed for each treatment. Data was analyzed from gut surgical specimens procured from 3 human subjects for each parameter; 12 Z-stacks in different networks of ganglia (nhMPG networks) in each patient were used for colocalization analysis and statistics. Statistical significance was determined by one-way ANOVA, followed by a post hoc Tukey's test. Values are expressed as mean ± SEM. *P < 0.05, **P < 0.01, ***P < 0.001; ns, not significant. Scale bars: 50 µm (A and B); 10 µm (I).

Figure-8

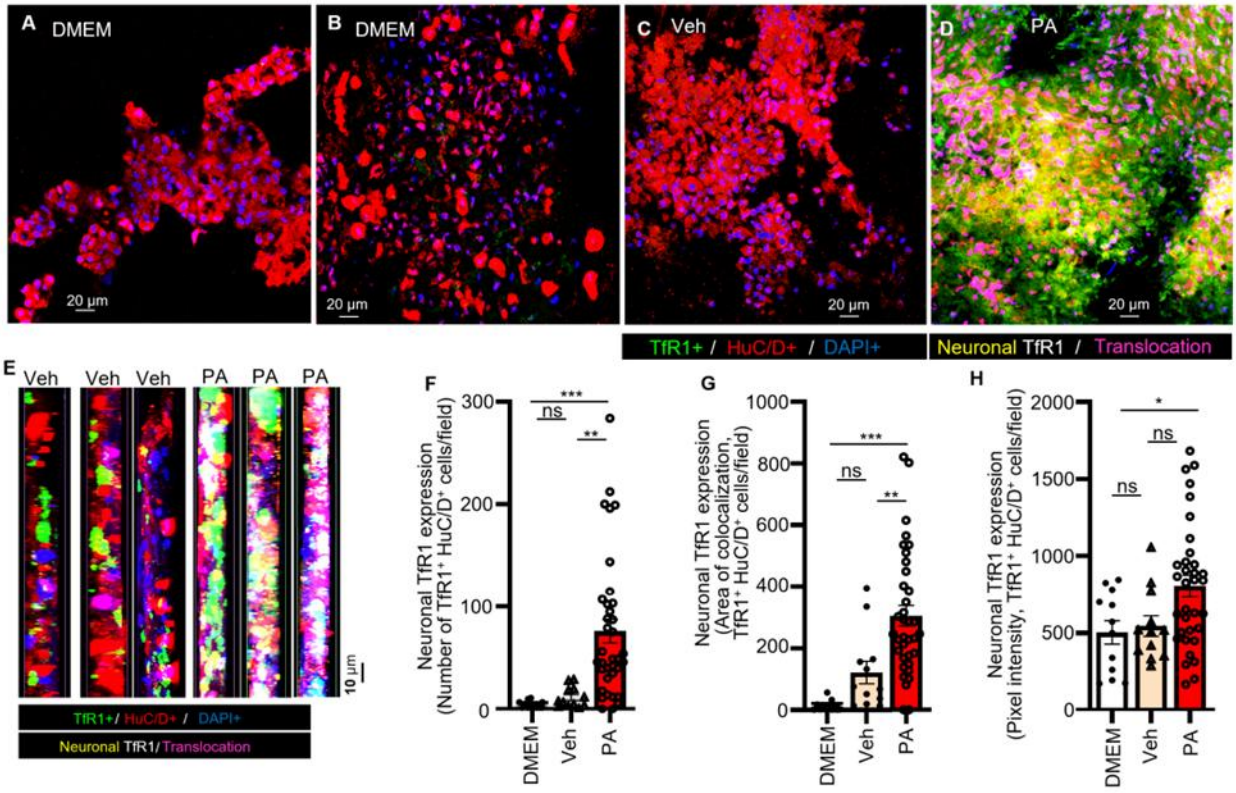

Figure 8. PA induction of Transferrin Receptor-1 (TfR1) expression in human myenteric neurons of nhMPG networks. Networks of human myenteric ganglia (nhMPG) isolated from surgical specimens were treated ex vivo with PA, DMEM, or vehicle control to assess neuronal TfR1 expression. (A-E) PA increased TfR1 expression in HuC/D+ neurons of hMPG networks, compared to DMEM or vehicle control. (E) Images shown are cross-sections of z-stack images through the networks of ganglia, to further illustrate neuronal TfR1. (F-H) PA caused an increase in the number of neurons/fields that expressed TfR1, the area of co-localization of TfR1 and HuC/D+ neurons/field, and it increased TfR1 expression (pixel intensity/field). Statistics: one-way ANOVA with Tukey's multiple-comparisons test. Data are mean ± SEM. *P < 0.05; **P < 0.01; ***P < 0.001; ns, not significant.

Figure-9

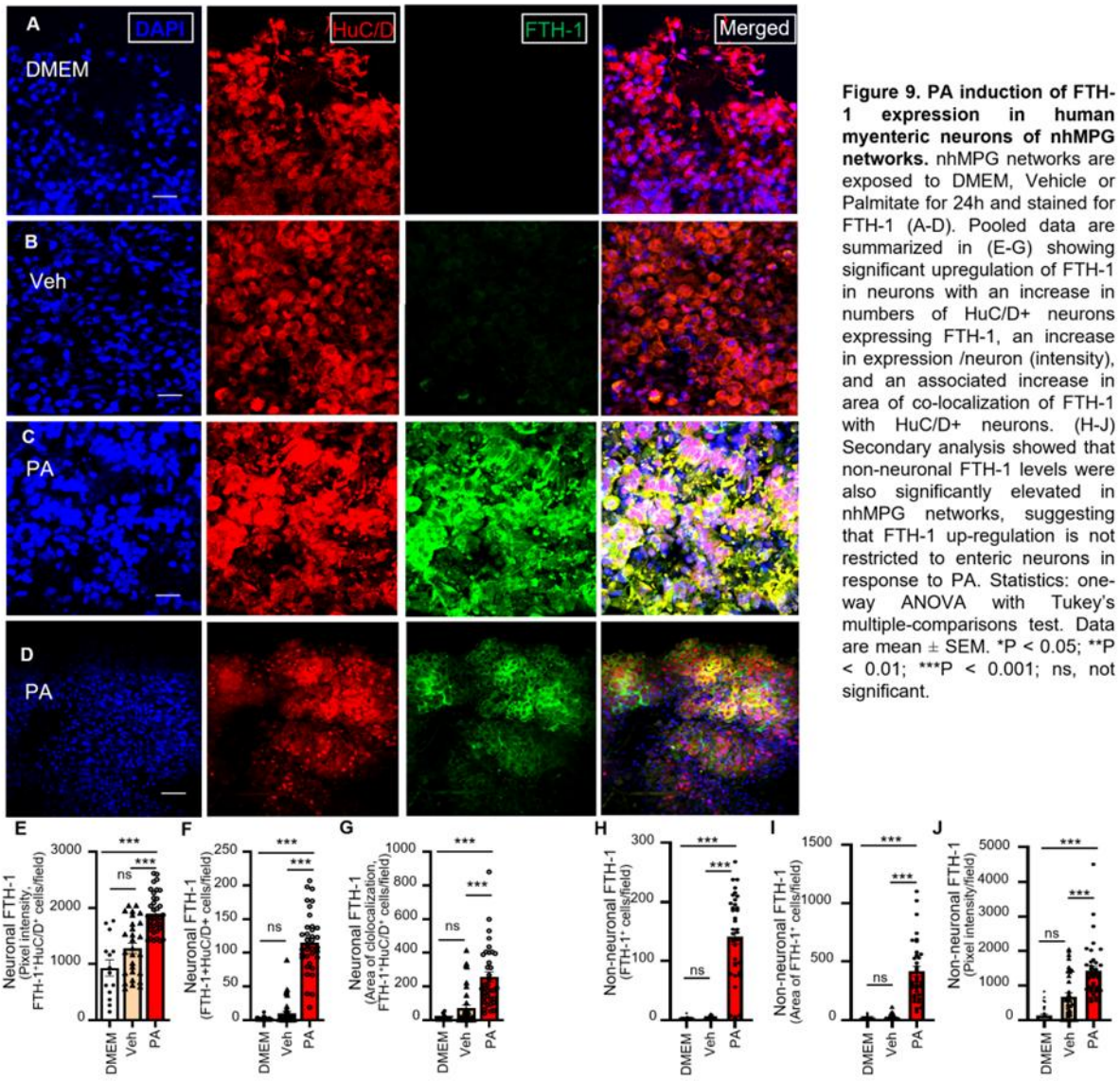

Figure 9. PA induction of FTH-1 expression in human myenteric neurons of nhMPG networks. nhMPG networks are exposed to DMEM, Vehicle or Palmitate for 24h and stained for FTH-1 (A-D). Pooled data are summarized in (E-G) showing significant upregulation of FTH-1 in neurons with an increase in numbers of HuC/D+ neurons expressing FTH-1, an increase in expression /neuron (intensity), and an associated increase in area of co-localization of FTH-1 with HuC/D+ neurons. (H-J) Secondary analysis showed that non-neuronal FTH-1 levels were also significantly elevated in nhMPG networks, suggesting that FTH-1 up-regulation is not restricted to enteric neurons in response to PA. Statistics: one-way ANOVA with Tukey's multiple-comparisons test. Data are mean ± SEM. *P < 0.05; **P < 0.01; ***P < 0.001; ns, not significant.

Figure-10

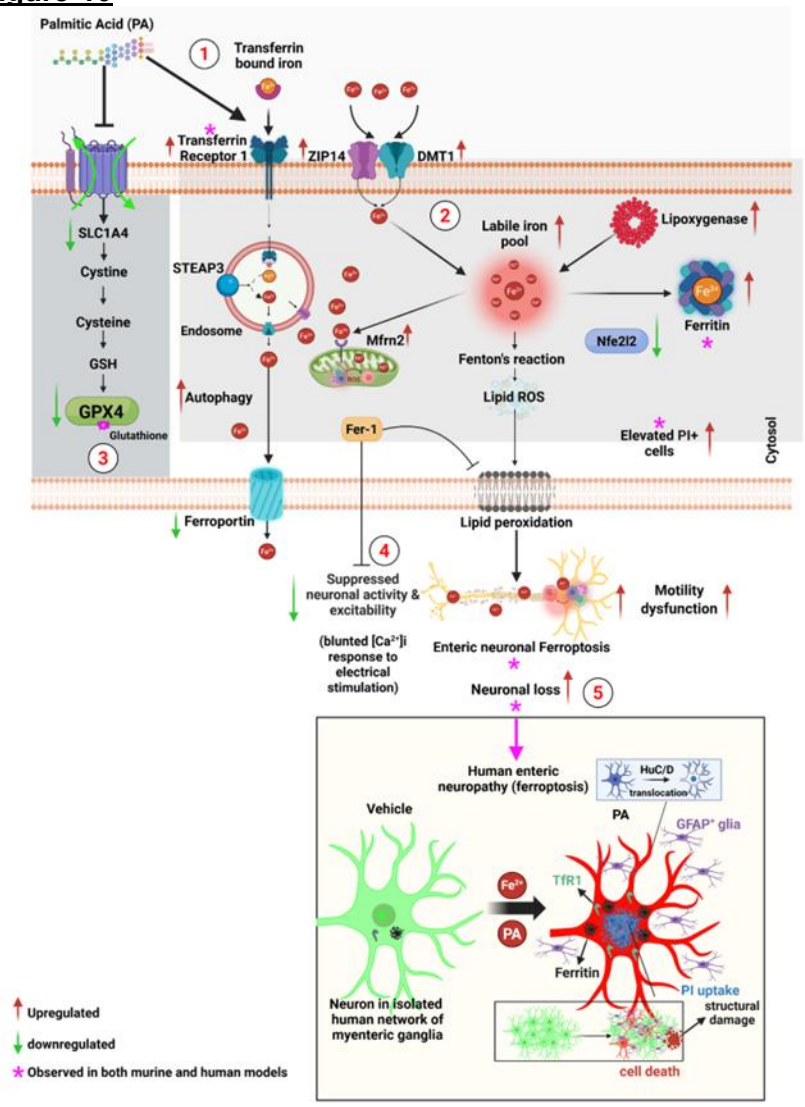

Figure 10. PA induces ferroptotic enteric neurodegeneration through iron accumulation, oxidative stress, and mitochondrial dysfunction in murine and human models. Schematic summary of the proposed mechanism by which chronic palmitic acid (PA), a major dietary saturated fatty acid, drives ferroptotic injury in enteric neurons, integrating findings from murine models and human networks of myenteric ganglia (nhMPG). Numbered steps: (**1**) Chronic PA exposure. (**2**) Increased iron uptake and trafficking through upregulation of transferrin receptor 1 (TfR1), divalent metal transporter 1 (DMT1), and ZIP14, expanding the intracellular labile Fe^{2+} pool and promoting iron retention. (**3**) Impaired antioxidant defense via suppression of cystine transport and the glutathione (GSH)-GPX4 axis, further sensitizing neurons to oxidative injury. (**4**) Functional ENS impairment, shown as suppressed neuronal activity and excitability (blunted intracellular free calcium $[Ca^{2+}]i$ response to electrical stimulation). (**5**) Convergent iron-driven oxidative stress and lipid peroxidation culminate in enteric neuronal ferroptosis and cell death, leading to neuronal loss and motility dysfunction. Fer-1 inhibits lipid peroxidation and preserves neuronal activity and excitability, mitigating ferroptotic cell death. Created with BioRender. Balasubramaniam, A. (2025).